AGU PUBLICATIONS

Geochemistry, Geophysics, Geosystems

RESEARCH ARTICLE
10.1002/2014GC005262

Key Points:
- The Makran arc magmatism might have started at ~19 Ma
- The arc magmas were derived from a subduction-modified, enriched mantle source
- The Makran represents a window between two continental collision zones

Supporting Information:
- ReadMe
- Text01
- Tables S1–S3

Correspondence to:
K.-N. Pang,
knpang@ntu.edu.tw

Citation:
Pang, K.-N., S.-L. Chung, M. H. Zarrinkoub, H.-Y. Chiu, and X.-H. Li (2014), On the magmatic record of the Makran arc, southeastern Iran: Insights from zircon U-Pb geochronology and bulk-rock geochemistry, *Geochem. Geophys. Geosyst.*, *15*, 2151–2169, doi:10.1002/2014GC005262.

Received 24 JAN 2014
Accepted 27 APR 2014
Accepted article online 2 MAY 2014
Published online 4 JUN 2014

On the magmatic record of the Makran arc, southeastern Iran: Insights from zircon U-Pb geochronology and bulk-rock geochemistry

Kwan-Nang Pang[1], Sun-Lin Chung[1], Mohammad Hossein Zarrinkoub[2], Han-Yi Chiu[1,3], and Xian-Hua Li[4]

[1]Department of Geosciences, National Taiwan University, Taipei, Taiwan, [2]Department of Geology, University of Birjand, Birjand, Iran, [3]Department of Physics and Earth Sciences, University of the Ryukyus, Okinawa, Japan, [4]State Key Laboratory of Lithospheric Evolution, Institute of Geology and Geophysics, Chinese Academy of Sciences, Beijing, China

Abstract Twenty-one magmatic rocks were analyzed for major and trace elements, and a subset of them for Sr-Nd isotopes and zircon U-Pb isotopes, to constrain magma genesis and tectonic evolution of the Makran arc, southeastern Iran. Representative samples from the Bazman and Taftan volcanoes yield zircon U-Pb ages from ~0.84 to ~7.5 Ma, consistent with published ages ranging from the Late Miocene to Late Pleistocene. The Mirabad granitic pluton adjacent to and geochemically similar to the Taftan volcano was dated at ~19 Ma, indicating that arc magmatism might have started earlier than commonly thought in the Early Miocene. The studied rocks show basaltic to rhyolitic compositions, calc-alkaline affinity, and an orogenic signature involving enrichments in large ion lithophile elements, light rare earth elements, Th and Pb, and depletions in high field strength elements and P, relative to elements of similar incompatibilities. The trace element ratios in a subset of relatively primitive samples are consistent with derivation from a mantle source that underwent subduction-related enrichment. The covariations of Sr and Nd isotopic ratios, and of these ratios and MgO and SiO_2, are consistent with combined assimilation and fractional crystallization. The process is modeled using covariations of $^{87}Sr/^{86}Sr$ and Sr concentration in the studied rocks given that Sr behaves as neutral or slightly incompatible. We propose, in light of published and our new data, that the Makran represents a window of continental collision between the India-Eurasia collision zone to the east and the Arabia-Eurasia collision zone to the west.

1. Introduction

A fundamental step in unraveling the complex geodynamic history of orogenic belts is the establishment of magmatic records, which involve careful sampling, precise age determination, and geochemical characterization of magmatic products in a given region [e.g., *Lustrino et al*., 2011; *Seghedi and Downes*, 2011; *Prelević and Seghedi*, 2013]. This paper investigates the petrogenesis and tectonic implications of a suite of magmatic rocks from the Makran arc, southeastern Iran, which is located in a poorly studied segment within the Alpine-Himalayan orogenic belt. The arc, which spans across southeastern Iran and southwestern Pakistan, is the surface expression of a ~1000 km long subduction system situated between the India-Eurasia collision zone and the Arabia-Eurasia collision zone [*McCall*, 1997, 2002]. Its volcanic activity is manifested by a linear belt of three large eruptive centers including the Taftan and Bazman volcanoes in southeastern Iran, and the Koh-i-Saltan volcano in southwestern Pakistan, and many small eruptive centers between them. Sparse K/Ar and $^{39}Ar/^{40}Ar$ age data for rocks from the above volcanoes indicate an age range from the Late Miocene to Quaternary, a period generally taken as indicative of active arc magmatism. However, most previous investigations of the Makran arc have focused on its structure and seismicity [*Byrne et al*., 1992; *Kopp et al*., 2000; *Grando and McClay*, 2007; *Regard et al*., 2010; *Smith et al*., 2012, 2013], and geochemical characterization of its magmatic rocks has not been systematically performed. In this study, we attempt to develop, together with published data, a magmatic record for the Makran arc using zircon U-Pb geochronology, bulk-rock elemental, and Sr-Nd isotopic geochemistry for a suite of magmatic rocks collected in the vicinity of the Taftan and Bazman regions, southeastern Iran. Our objectives are to better understand (i) the timing and duration of arc magmatism, (ii) the petrogenetic processes responsible for any geochemical variations among the arc rocks, and (iii) the tectonic implications associated with the formation of the arc.

2. Background

2.1. Regional Geology

The paleogeographic and tectonic evolution of Iran was presented in detail by *Stöcklin* [1968], *Berberian and King* [1981], and *Ramezani and Tucker* [2003], and only a brief summary is given here. As part of the Alpine-Himalayan orogenic system, Iran consists of a tectonic collage of Gondwana-derived terranes that had been successively accreted to the southern margin of Eurasia [*Dewey et al*., 1973; *Şengör et al*., 1988; *Alavi*, 1994; *Şengör and Natal'in*, 1996]. The terrane collision resulted in the obduction of ophiolitic rocks [*Ghazi et al*., 2004] and the development of mountain ranges including the Alborz-Kopeh Dagh ranges in northern Iran, the Zagros ranges in southwestern Iran, and the east Iranian ranges. The mountain ranges are juxtaposed with major suture zones, for example, a Paleotethyan suture along the Alborz-Kopeh Dagh ranges [*Alavi et al*., 1997], the Bitlis-Zagros suture along the Zagros ranges [*Agard et al*., 2011, and references therein], and the Sistan suture along the east Iranian ranges [*Tirrul et al*., 1983; *McCall*, 1997] (Figure 1a, inset). The latter two sutures are Neotethyan in nature; the north-south-trending Sistan suture marks the collision between the Lut and Afghan (or Helmand) microcontinental blocks in the Late Cretaceous [*Zarrinkoub et al*., 2012; *Angiboust et al*., 2013] whereas the Bitlis-Zagros suture records the collision of Arabia to Eurasia, or any terranes accreted to its southern margin, since the Late Eocene-Early Oligocene [*Allen and Armstrong*, 2008; *Agard et al*., 2011; *Ballato et al*., 2011; *McQuarrie and van Hinsbergen*, 2013; *McQuarrie et al*., 2003]. Surrounded by the aforementioned mountain ranges is a region of moderate relief known as the central Iranian microcontinent containing, from east to west, the Lut, Tabas, and Yazd blocks (Figure 1a, inset). In southeastern Iran, the east-west-trending Makran ranges extend to southwestern Pakistan [*McCall*, 1997].

The oldest magmatic rocks in Iran have Late Neoproterozoic to Early Cambrian ages (~590–500 Ma) and have been related to an orogenic event along the Proto-Tethyan margin of the Gondwanaland [*Ramezani and Tucker*, 2003; *Hassanzadeh et al*., 2008; *Azizi et al*., 2011; *Chiu et al*., 2013]. During the Paleozoic, magmatism appeared to be largely inactive or of very limited extent throughout the country. From the Early Mezosoic to Late Cenozoic, extensive magmatism related to Neotethyan subduction was preserved in two magmatic belts subparallel to the Bitlis-Zagros suture: one dominated by Jurassic-Cretaceous granitic plutons and volcanic rocks in the Sanandaj-Sirjan zone [*Stöcklin*, 1968] and another dominated by Paleogene volcanic rocks, i.e., the Urumieh-Dohktar magmatic arc (UDMA) [*Schroder*, 1944; *Alavi*, 1994]. The Paleogene magmatic activity was confined not only to the UDMA but also along the Alborz ranges and in the Lut-Sistan region, together representing a period of magmatic flare-up [*Berberian and King*, 1981; *Camp and Griffis* 1982; *Jung et al*., 1983; *Verdel et al*., 2011; *Pang et al*., 2013a]. Magmatic activity from the Miocene to Quaternary appeared to be less extensive compared to the Paleogene pulse and was confined to isolated volcanic centers in northwestern Iran [e.g., *Kheirkhah et al*., 2009; *Aghazadeh et al*., 2010; *Allen et al*., 2013; *Pang et al*., 2013b], northern Iran [*Davidson et al*., 2004], northeastern Iran (Quchan), eastern Iran [*Walker et al*., 2009; *Pang et al*., 2012], and southeastern Iran [*Saadat and Stern*, 2011, this study], and some volcanic centers and small plutons along the UDMA [*Jahangiri*, 2007; *Omrani et al*., 2008; *Chiu et al*., 2013]. A wide range of magma types with ultrapotassic, adakitic, alkali basaltic, calc-alkaline, and shoshonitic compositions has been identified for the Miocene-Quaternary magmatism.

2.2. Geology of the Makran Subduction System

The Makran of Iran and Pakistan is an active arc system where the oceanic portion of the Arabian Plate subducts toward the north beneath Eurasia at a rate of ~2 cm per year [*Farhoudi and Karig*, 1977; *Verdant et al*., 2004]. It consists of a trench (i.e., the Makran trench) running roughly east-west at ~24°N–25°N offshore in the Gulf of Oman, an extensive (~1000 km × 350 km) and one of the world's largest accretionary prism [*Platt et al*., 1985; *Kopp et al*., 2000; *Grando and McClay*, 2007], the subaerial portion of which is referred to as the Makran ranges, and a chain of arc volcanoes aligned in an ENE-WSW orientation further inland (i.e., the Makran arc). The eastern limit of the Makran is the sinistral Ornach-Nal and Chaman faults, the boundary between the Eurasian and the Indian plates continuing toward the Indus-Yarlung suture. To the west, the Makran passes into the Zagros ranges through the dextral Zendan-Minab-Palami fault system, which extends toward the Bitlis-Zagros suture (or the Main Zagros Thrust), the plate boundary between Arabia and Eurasia [*Regard et al*., 2010]. Situated to the north of Makran is the north-south-trending Sistan suture zone separating the Lut block to the west and the Afghan block to the east.

A comprehensive review on the geology of the Iranian Makran is given by *McCall* [1997, 2002]. The age of the subducting Arabian Plate was inferred to be either Jurassic or older [*Whitmarsh*, 1979] or Eocene

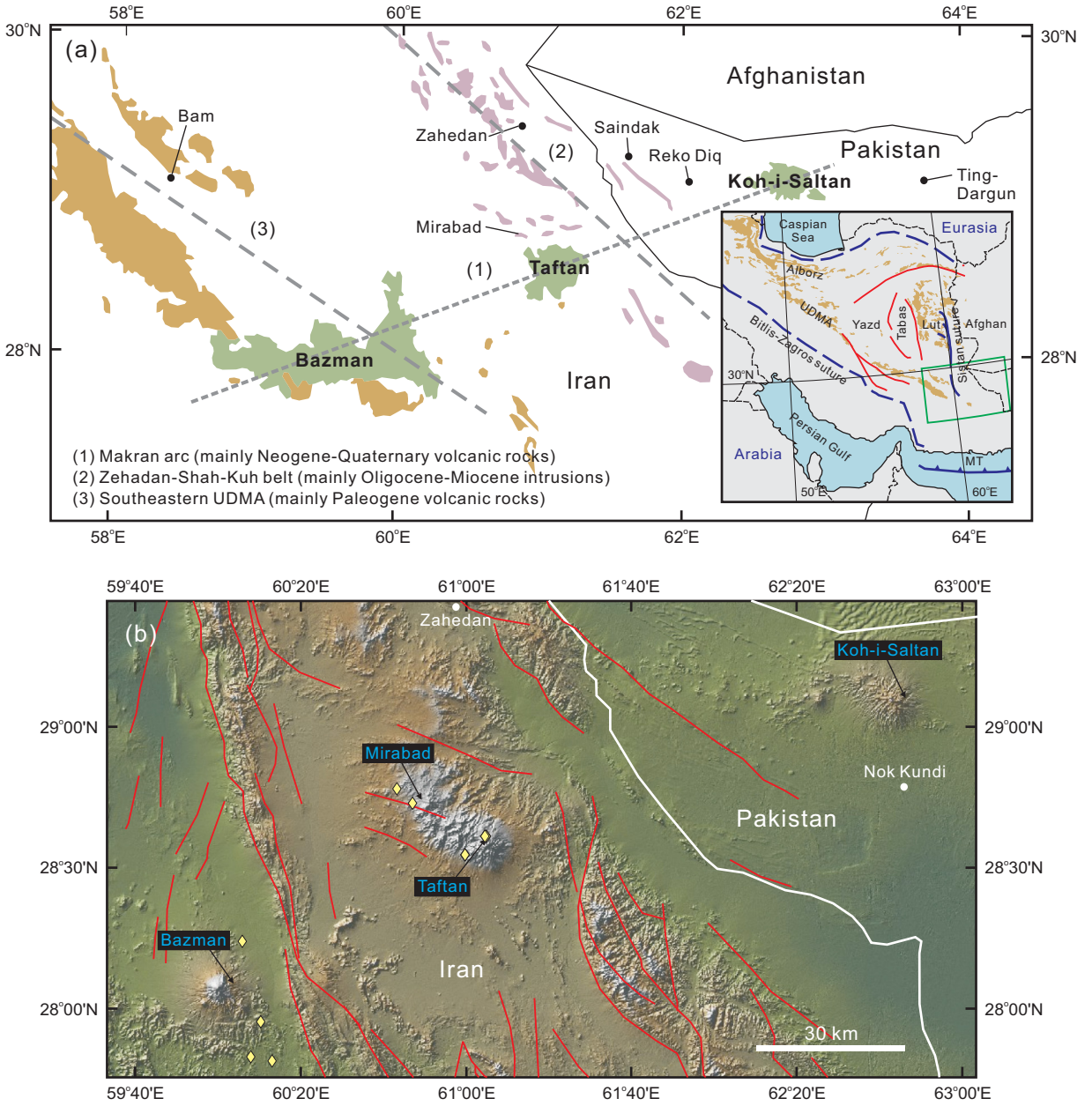

Figure 1. (a) A simplified geological sketch map of the Makran region showing three large volcanoes of the Makran arc including Bazman, Taftan, and Koh-i-Sultan, the southeastern part of the Urumieh-Dokhtar magmatic arc and the Zahedan-Shah Kuh plutonic belt. It is noteworthy that the latter two belts are at an acute angle to the Makran arc. Inset shows the study area in southeastern Iran (green frame) and the distribution of Paleogene volcanic rocks in the country. MT = Makran trench. (b) A satellite image of the same region taken from the software GeoMapApp (http://www.geomapapp.org). Red lines denote major faults after *Richards et al.* [2012]. Yellow symbols denote sampling sites.

[*Mountain and Prell*, 1990]; the heat flow data by *Hutchison et al.* [1981] are consistent with the older age. The Makran subduction system is associated with several characteristic features including high sediment input [*Platt et al.*, 1985], gentle dip of the downgoing slab [*Byrne et al.*, 1992], and low historical seismicity [*Byrne et al.*, 1992]. The thickness of the incoming sediments is up to 5–7 km, most of which were accreted to form the accretionary prism and the rest of them might have been transported to greater depths with the subducting slab [*Platt et al.*, 1985; *Kopp et al.*, 2000; *Grando and McClay*, 2007]. The source of sediments was likely to be the proto-Indus fan with accumulated sediments from the Himalayas [*Garzanti et al.*, 1996], in addition to those eroded from the Makran continental margin. The long arc-trench distance (400–600 km) and seismological data are indicative of a shallow-dipping (2–8°) Benioff zone [*Byrne et al.*, 1992; *Kopp*

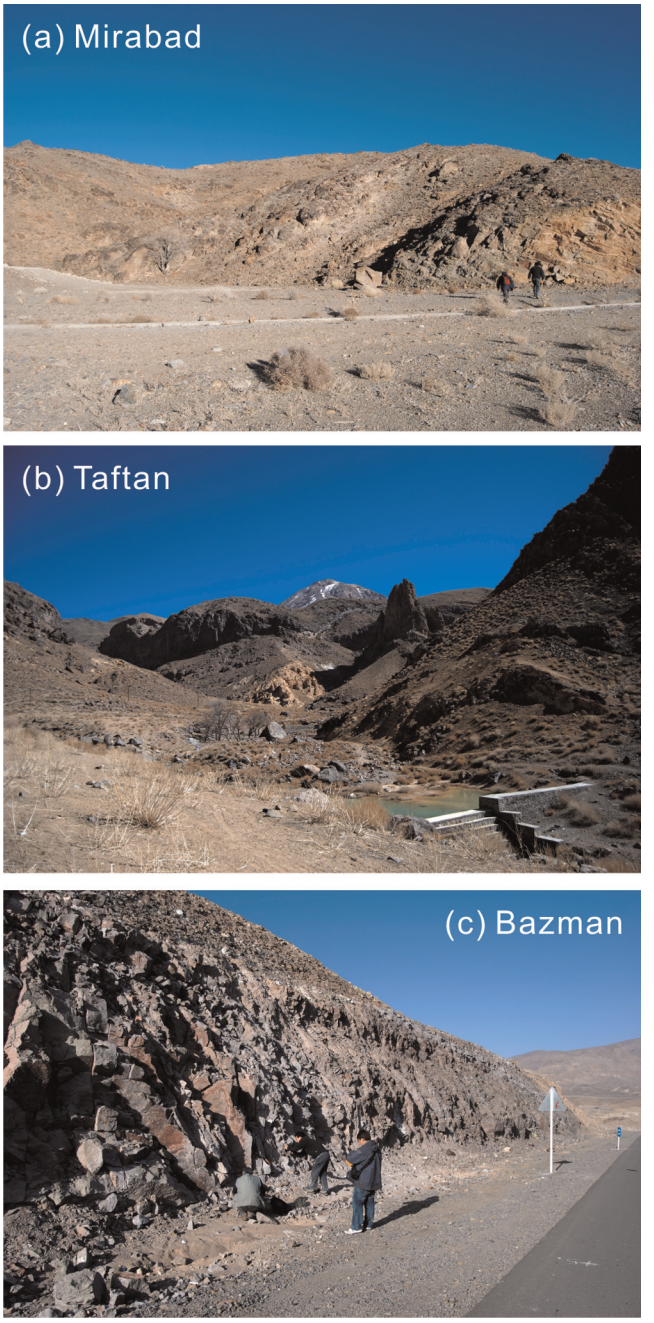

Figure 2. Field occurrences of selected sampling sites in this study. (a) A roadcut section exposing granitic rocks at Mirabad along the highway between Zahedan and Khash. (b) An outcrop on the Taftan volcano (its summit is the icy peak in the upper central part of the photograph). (c) A roadcut section near the foot of the Bazman volcano.

et al., 2000]. The generally low seismicity of the Makran, especially for its western part, might be attributable to the presence of an appreciable quantity of young and poorly consolidated sediments, which are resistant to accelerating slip associated with earthquakes [*Marone and Scholz*, 1988], on the subducting slab.

The Makran arc consists of three stratovolcanoes including, from east to west, the Koh-i-Sultan in Pakistan, and the Taftan and Bazman in Iran (Figure 1a), and numerous smaller volcanic centers in between them. The fact that they form an ENE-WSW chain at an angle to the Makran trench has been ascribed to different dips of the subducting slab east and west of the Sonne fault, along which the Ormara microplate was torn from the eastern edge of the Arabian plate [*Kukowski et al*., 2000]. All three volcanoes are dominated by lavas and pyroclastic rocks of andesitic to dacitic composition with minor basalts and basaltic andesites. The Koh-i-Saltan volcano is located on the Afghan block with a maximum elevation of ~2300 m. *Richards et al*. [2012] dated one andesite sample at ~5.6 Ma by $^{40}Ar/^{39}Ar$ step-heating technique. The Taftan volcano is located in the southern Sistan suture zone and its summit is ~4050 m in height. *Biabangard and Moradian* [2008] obtained K/Ar ages of ~7.0 Ma for a basalt sample, and ~6.0 and ~0.7 Ma for two andesite samples. The Bazman volcano is situated on the southern part of the Lut block with a maximum elevation of ~3500 m. *Conrad et al*. [1981] dated three basalt samples near the volcano at ~11.5, ~4.7, and ~0.7 Ma using the K/Ar method.

3. Sampling and Analytical Methods

Twenty-one samples of igneous rocks were collected in the Makran region, southeastern Iran (Figure 1b), including two from the Mirabad pluton (Figure 2a), nine from the Taftan volcano (Figure 2b), and ten near the Bazman volcano (Figure 2c). Representative samples were selected for zircon U-Pb dating by laser ablation (LA)-inductively coupled plasma-mass spectrometry (ICP-MS) in Department of Geosciences, National

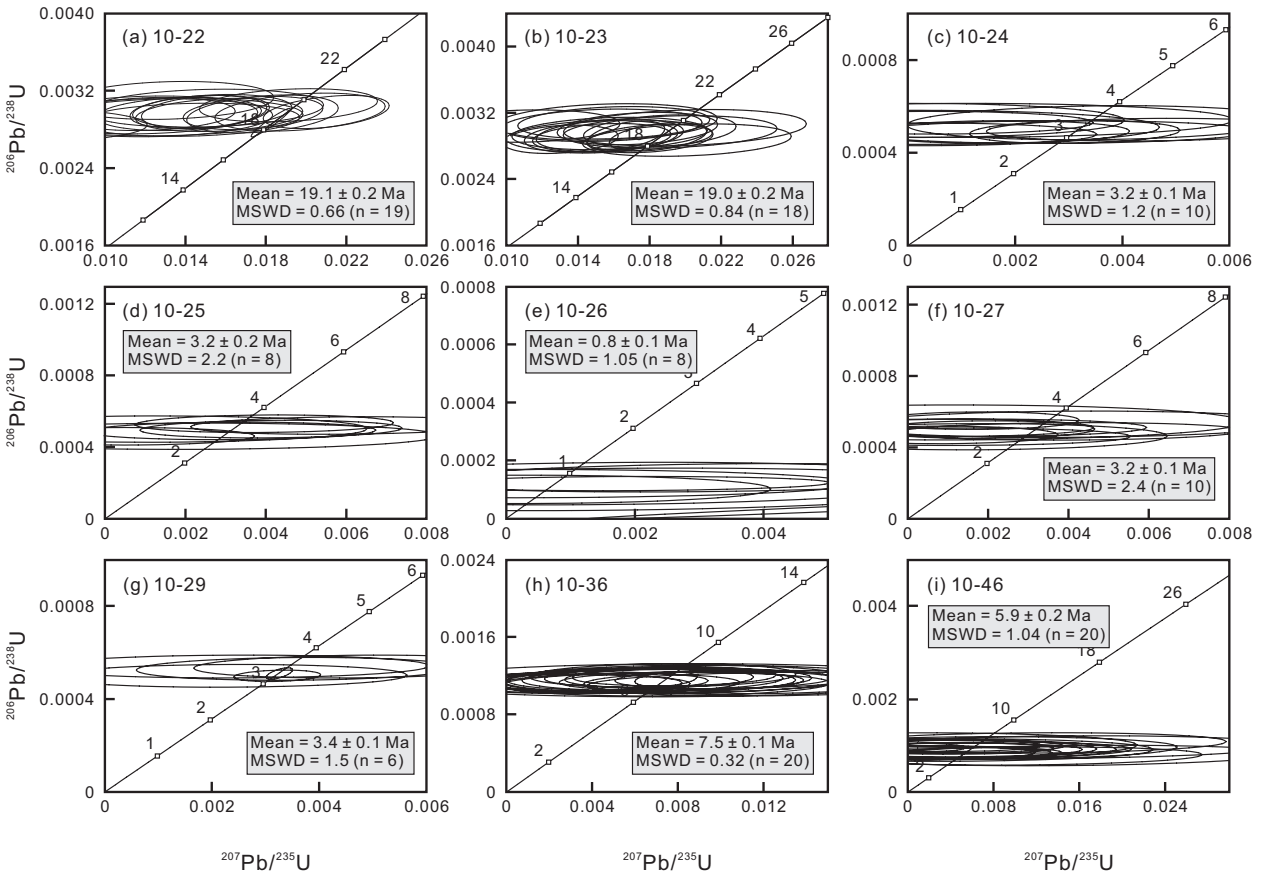

Figure 3. Conventional U-Pb concordia diagrams for nine zircon samples dated by LA-ICP-MS. (a) 10–22; (b) 10–23; (c) 10–24; (d) 10–25; (e) 10–26; (f) 10–27; (g) 10–29; (h) 10–36; and (i) 10–46. The mean values denote mean $^{206}Pb/^{238}U$ ages with 2σ errors. MSWD = mean square weighted deviation; n = number of analyzed spots.

Taiwan University, Taiwan and secondary ion mass spectrometry (SIMS) in Institute of Geology and Geophysics, Chinese Academy of Sciences, Beijing, China. The results of LA-ICP-MS and SIMS analyses are illustrated in Figures 3 and 4, and the full analytical data are given in supporting information. All samples were measured for loss on ignition (LOI), major, and trace elements, and a subset of them for Sr-Nd isotopes in Department of Geosciences, National Taiwan University, Taiwan. Measurements were made on rock powders, which were carefully prepared by cutting, crushing, and pulverization in agate mortars to minimize potential contamination of transition elements in trace element analyses. The analytical procedures are described in further detail in supporting information.

4. Results

4.1. The Mirabad Pluton

According to the QAPF modal classification of plutonic rocks [*Streckeisen*, 1976], samples 10–22 and 10–23 from the Mirabad pluton are classified as granodiorite. They are dated at 19.1 ± 0.2 and 19.0 ± 0.2 Ma by LA-ICP-MS zircon U-Pb technique (Figures 3a and 3b). On a plot of K_2O versus SiO_2 [*Peccerillo and Taylor*, 1976], they show high-K calc-alkaline affinity and represent intrusive equivalents of high-K andesite and high-K dacite (Figure 5a). Sample 10–22 has a molar (Na + K)/Al value of 0.51 and an aluminum saturation index (ASI) of 0.95 and is thus metaluminous. Sample 10–23 has an identical molar (Na + K)/Al value but an ASI of 1.05 and is slightly peraluminous. The primitive mantle-normalized trace element patterns for both samples are characterized by enrichments of large ion lithophile elements (LILE) and light rare earth elements (LREE), a prominent Pb spike and Nb-Ta-Ti-P troughs (Figure 7a). Such an orogenic signature is commonly observed in rocks of the upper continental crust [*Rudnick and Gao*, 2003] and in arc magmas [*Gill*,

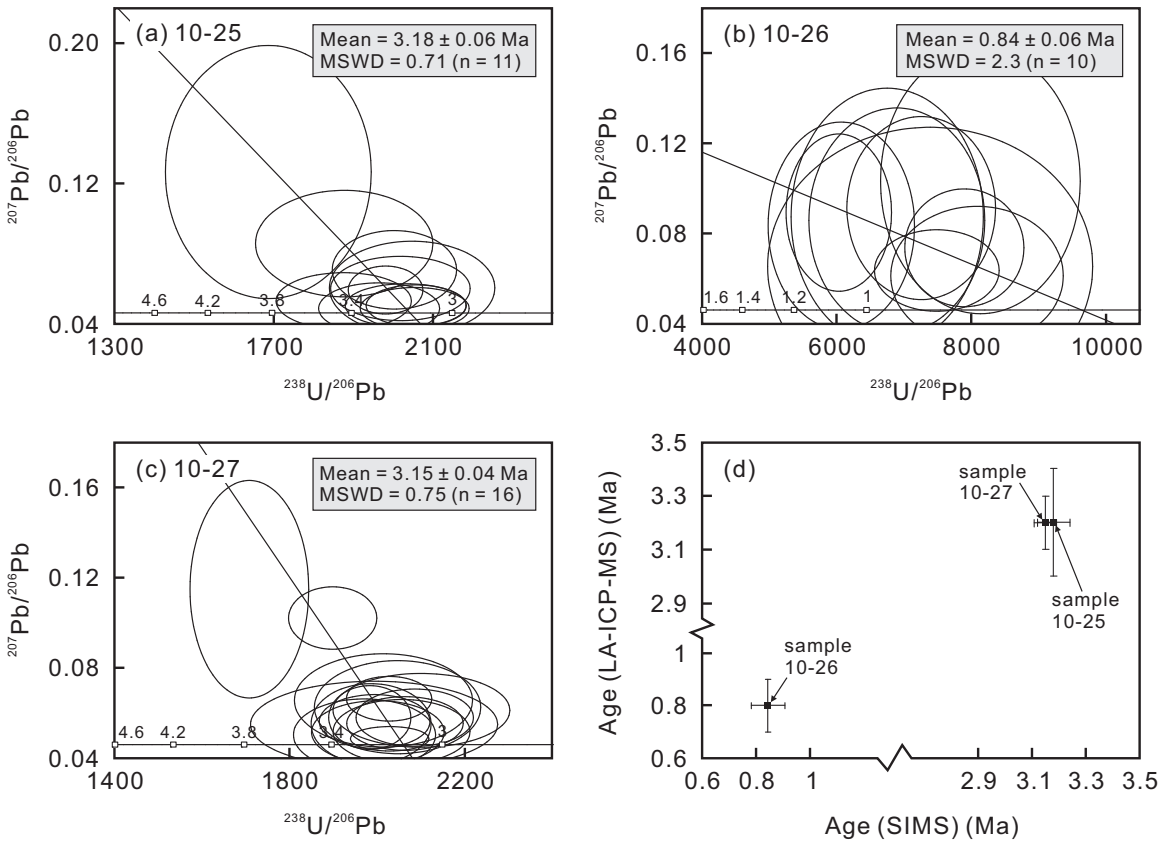

Figure 4. Tera-Wasserburg concordia diagrams for three zircon samples dated by SIMS. (a) 10–25; (b) 10–26; and (c) 10–27. (d) Comparison of zircon U-Pb age results for samples dated by both LA-ICP-MS and SIMS. The mean values in Figures 4a–4c denote ^{207}Pb-corrected $^{206}Pb/^{238}U$ ages with 2σ errors. MSWD = mean square weighted deviation; n = number of analyzed spots.

1981; *Thorpe*, 1982; *Tatsumi*, 1989; *Pearce and Peate*, 1995]. The two Mirabad samples have $^{87}Sr/^{86}Sr$ of 0.7076 and 0.7084, and $^{143}Nd/^{144}Nd$ of 0.5123 and 0.5124, which are more enriched than the Bulk Silicate Earth (Figure 8 and Table 1).

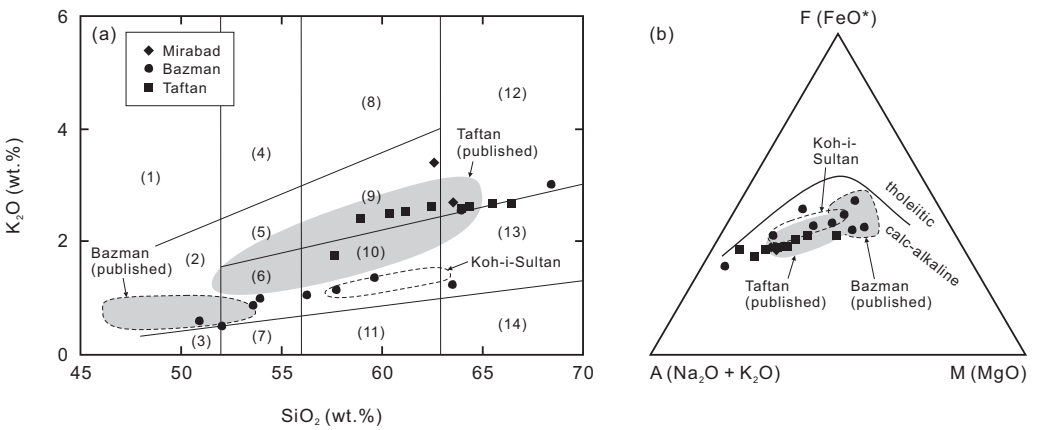

Figure 5. Diagrams illustrating rock classification in this study. (a) A binary plot of K_2O versus SiO_2 [after *Peccerillo and Taylor*, 1976]. Four common rock series include: the low-K series (low-K tholeiite (3), low-K basaltic andesite (7), low-K andesite (11), and low-K dacite (14)), the medium-K series (basalt (2), basaltic andesite (6), andesite (10), and dacite (13)), the high-K series (basalt (2), high-K basaltic andesite (5), high-K andesite (9), and high-K dacite (12)), and the shoshonitic series (absarokite (1), shoshonite (4), and banakite (8)). (b) A ternary plot of ($Na_2O + K_2O$)–FeO*–MgO (the AFM diagram) [*Kuno*, 1968]. FeO* denotes the amount of total iron oxides assuming $Fe_2O_3/FeO = 1:9$. Reference fields for Neogene-Quaternary magmatic rocks at Bazman (Iran), Taftan (Iran), and Koh-i-Sultan (Pakistan) are drawn after published data by *Biabangard and Moradian* [2008], *Saadat and Stern* [2011], and *Richards et al.* [2012].

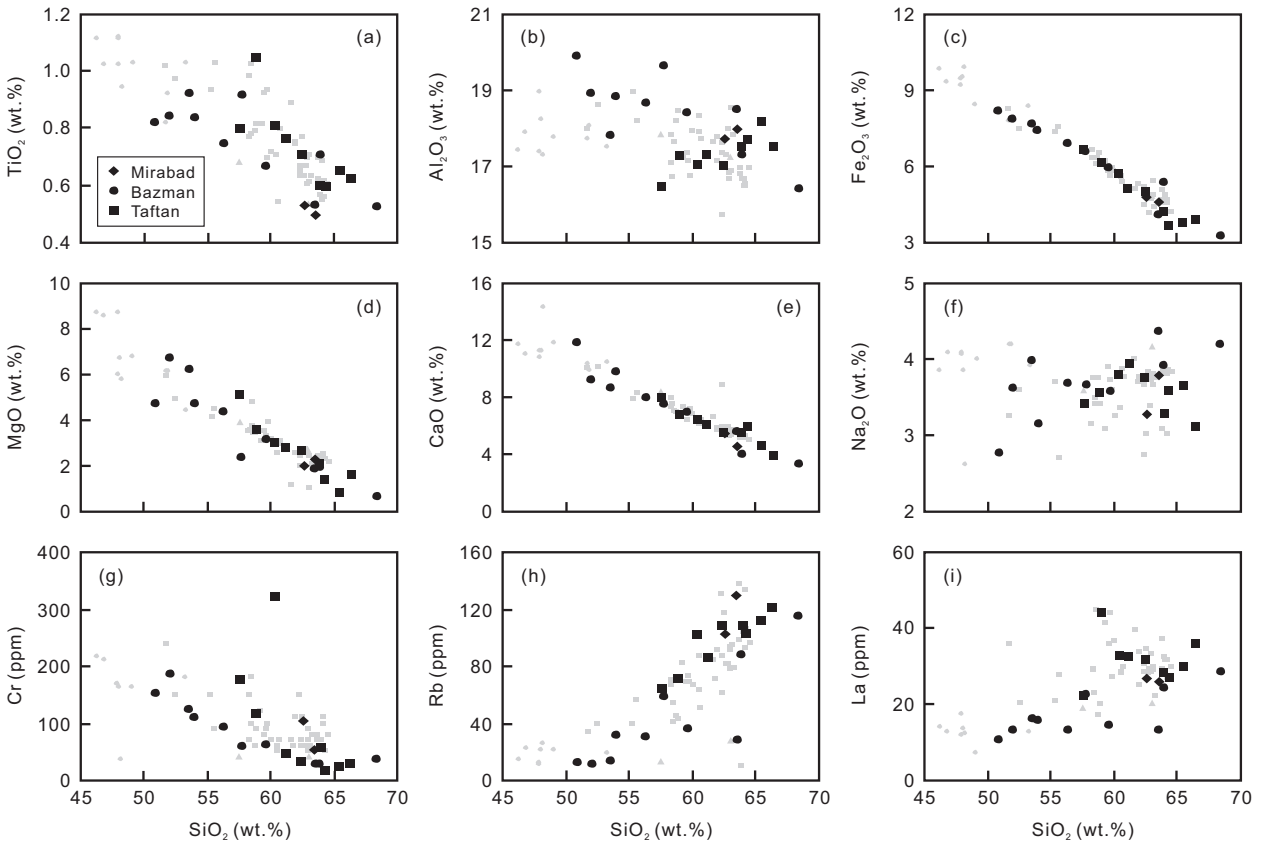

Figure 6. Binary diagrams illustrating the elemental variations versus SiO_2 concentrations in the studied rocks. (a) TiO_2; (b) Al_2O_3; (c) total iron as Fe_2O_3; (d) MgO; (e) CaO; (f) Na_2O; (g) Cr; (h) Rb; and (i) La. Gray symbols denote published data following the same legend as in Figure 6a, except triangular symbols standing for published data from the Koh-i-Sultan volcano.

4.2. The Taftan Volcano

Five samples from the Taftan volcano are dated by LA-ICP-MS zircon U-Pb technique at ~3.4 Ma (one sample), ~3.2 Ma (three samples), and ~0.8 Ma (one sample; Figures 3c–3g). Among these, zircon in samples 10–25, 10–26, and 10–27 is also analyzed by SIMS (Figures 4a–4c), yielding similar age results with higher precision (Figure 4d). The Taftan samples have intermediate to rhyolitic compositions (~56.1–63.9 wt % SiO_2) and their calc-alkaline affinity is evident in the K_2O-SiO_2 diagram [*Peccerillo and Taylor*, 1976] (Figure 5a) and the AFM diagram [*Kuno*, 1968] (Figure 5b). They are metaluminous to slightly peraluminous with molar (Na + K)/Al from 0.46 to 0.53 and ASI from 0.76 to 1.19. The SiO_2 concentrations vary positively with Al_2O_3 (~16.5–17.7 wt %), K_2O (~1.7–2.6 wt %), and Rb (~64–121 ppm) and negatively with TiO_2 (~0.57–1.0 wt %), Fe_2O_3 (~3.6–6.4 wt %), MgO (~0.8–4.9 wt %), CaO (~3.7–7.7 wt %), and Cr (~18–322 ppm; Figures 5, 6a–6e, 6g, and 6h). No systematic variation is observed between SiO_2 and Na_2O or La (Figures 6f and 6i). All samples show consistent primitive mantle-normalized trace element patterns characterized by an orogenic signature like the Mirabad samples (Figure 7b). In addition, the trace element data are in good agreement with those published by *Biabangard and Moradian* [2008] for the Taftan volcanic rocks. Most Taftan samples are characterized by high $^{87}Sr/^{86}Sr$ (0.7063–0.7068) and low $^{143}Nd/^{144}Nd$ (0.5124–0.5125) relative to the Bulk Silicate Earth, except sample 10–31 that has depleted Sr-Nd isotopic compositions ($^{87}Sr/^{86}Sr = 0.7044$, $^{143}Nd/^{144}Nd = 0.5128$; Figure 8 and Table 1).

4.3. The Bazman Volcano

Samples 10–36 and 10–46 in the vicinity of the Bazman volcano are dated by LA-ICP-MS zircon U-Pb technique at 7.5 ± 0.1 and 5.9 ± 0.2 Ma, respectively (Figures 3h and 3i). Ranging from basaltic to rhyolitic in composition, most Bazman samples belong to the medium-K calc-alkaline series, except two rhyolitic samples lying close to the boundary between the medium-K and high-K series on the K_2O-SiO_2 diagram (Figure 5a).

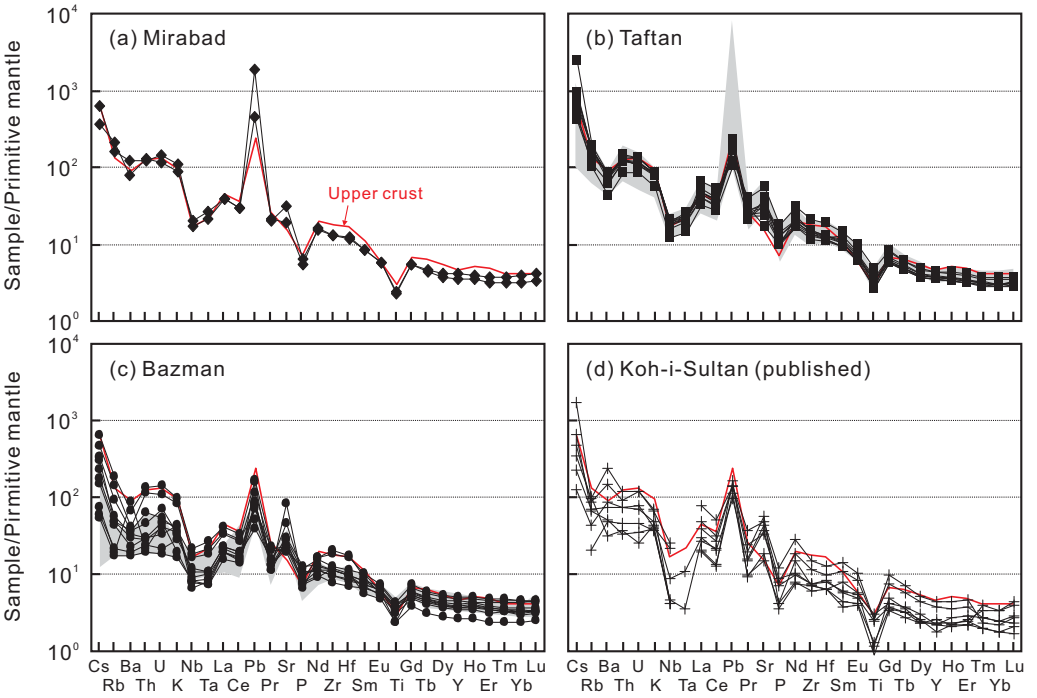

Figure 7. Primitive mantle-normalized trace element variation diagrams. (a) Mirabad; (b) Taftan; (c) Bazman; and (d) Koh-i-Sultan (published data). The red line denotes the pattern for the average elemental abundances of the upper continental crust [*Rudnick and Gao*, 2003]. Shaded areas in Figures 7b and 7c denote variations for published data. Normalizing values are after *Sun and McDonough* [1989].

The calc-alkaline affinity of the samples is also evident on the AFM diagram (Figure 5b). The intermediate to rhyolitic samples (>52 wt % SiO_2 on a volatile-free basis) are metaluminous to slightly peraluminous with molar (Na + K)/Al from 0.33 to 0.62 and ASI from 0.78 to 1.07. The SiO_2 concentrations (~50.4–68.1 wt %) of the samples correlate negatively with TiO_2 (~0.52–0.91 wt %), Al_2O_3 (~16.3–19.7 wt %),

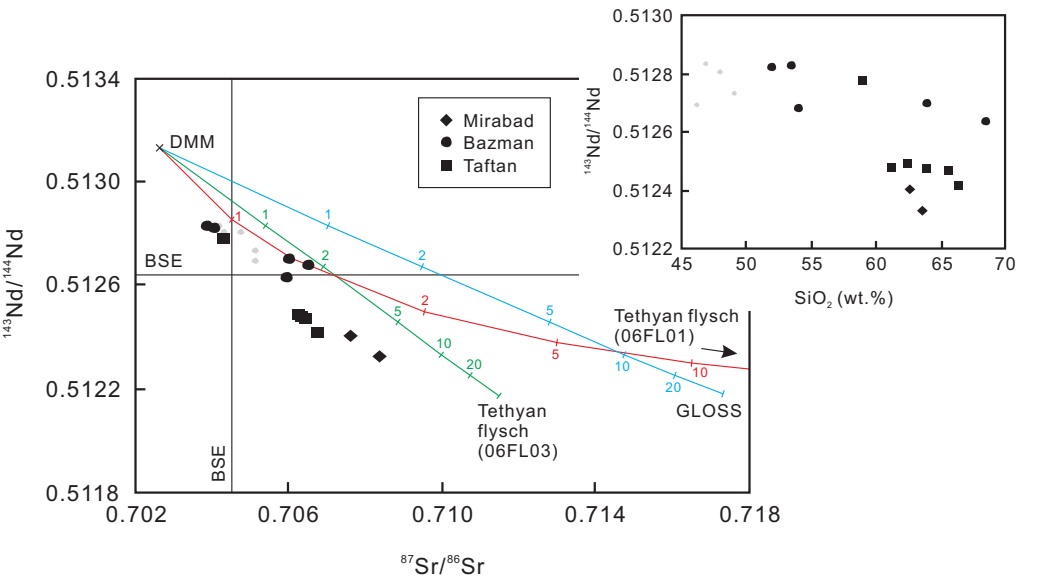

Figure 8. A binary plot of $^{143}Nd/^{144}Nd$ versus $^{87}Sr/^{86}Sr$. Inset shows a binary plot of $^{143}Nd/^{144}Nd$ versus SiO_2. The curves between depleted MORB mantle [*Workman and Hart*, 2005] and GLOSS [*Plank and Langmuir*, 1998] or Tethyan flysch [*Prelević et al.*, 2008] are binary mixing arrays, and the tick marks denote mixing percentages.

AGU Geochemistry, Geophysics, Geosystems

10.1002/2014GC005262

Table 1. Elemental and Sr-Nd Isotopic Data for the Makran Arc Rocks, Southeastern Iran

	Mirabad		Taftan									Bazman									
Sample	10–22	10–23	10–24	10–25	10–26	10–27	10–28	10–29	10–30	10–31	10–32	10–34	10–36	10–37	10–42	10–45	10–46	10–47	10–48	10–49	10–50
Major Oxides (wt %)																					
SiO_2	60.61	62.34	62.70	61.44	61.71	63.91	56.07	59.79	63.14	57.35	58.57	53.84	68.13	59.11	50.39	57.39	62.14	52.52	62.98	55.50	52.13
TiO_2	0.52	0.49	0.59	0.57	0.70	0.63	0.77	0.74	0.58	1.02	0.79	0.84	0.52	0.66	0.81	0.91	0.69	0.90	0.53	0.73	0.85
Al_2O_3	17.17	17.64	16.54	16.82	16.77	17.68	16.01	16.90	17.34	16.77	16.50	18.78	16.33	18.23	19.68	19.52	16.79	17.44	18.33	18.40	18.94
Fe_2O_3[a]	4.61	4.52	3.68	4.08	4.91	3.65	6.44	4.97	3.59	5.94	5.52	7.39	3.25	5.89	8.06	6.52	5.24	7.49	4.05	6.81	7.87
MnO	0.13	0.11	0.08	0.08	0.09	0.01	0.11	0.09	0.07	0.09	0.09	0.12	0.09	0.10	0.13	0.11	0.11	0.13	0.07	0.12	0.13
MgO	1.94	2.22	1.49	1.97	2.62	0.78	4.91	2.74	1.34	3.45	2.94	4.68	0.66	3.12	4.69	2.37	1.89	6.07	1.87	4.26	6.73
CaO	5.24	4.40	3.66	5.22	5.41	4.47	7.72	5.84	5.75	6.47	6.15	9.73	3.29	6.91	11.68	7.49	3.82	8.47	5.56	7.82	9.16
Na_2O	3.17	3.71	2.92	3.14	3.70	3.54	3.31	3.85	3.50	3.46	3.67	3.14	4.16	3.55	2.73	3.64	3.81	3.90	4.32	3.64	3.62
K_2O	3.28	2.64	2.51	2.48	2.56	2.60	1.70	2.46	2.57	2.32	2.40	0.98	2.98	1.32	0.58	1.12	2.47	0.84	1.22	1.03	0.50
P_2O_5	0.14	0.12	0.21	0.22	0.28	0.24	0.23	0.28	0.22	0.38	0.30	0.20	0.14	0.17	0.17	0.26	0.19	0.28	0.16	0.22	0.24
LOI	3.10	2.29	5.23	5.31	0.98	2.64	0.70	0.53	2.45	0.77	0.87	1.11	1.37	0.83	1.61	1.40	3.21	0.31	0.50	1.24	0.40
Total	99.89	100.48	99.62	101.32	99.71	100.15	97.97	98.19	100.54	98.01	97.79	100.80	100.92	99.88	100.52	100.72	100.37	98.33	99.59	99.76	100.55
Mg#[b]	45.4	49.3	44.5	48.9	51.3	29.7	60.2	52.2	42.4	53.5	51.4	55.6	28.8	51.2	53.6	41.8	41.7	61.6	47.7	55.3	62.9
Trace Elements (ppm)																					
Sc	6.66	12.1	13.1	4.61	6.95	0.41	19.6	11.1	3.70	18.2	13.0	20.7	7.98	16.0	25.7	19.6	15.2	13.2	4.13	8.66	13.8
V	64.6	40.7	61.3	58.1	76.8	64.3	123	63.6	57.4	113	88.1	176	47.3	114	194	121	60.4	119	51.9	105	125
Cr	105	54.2	26.9	55.0	31.9	22.8	175	44.2	18.1	115	322	109	37.4	61.5	151	59.0	27.8	123	28.6	92.3	187
Co	8.72	7.08	8.06	7.62	10.73	6.35	19.5	11.2	6.66	13.9	14.1	23.1	4.84	16.3	24.1	14.2	11.1	24.2	9.92	22.3	26.1
Ni	51.3	21.1	15.5	30.0	21.3	16.4	69.2	25.0	11.8	54.6	166	56.5	19.0	46.2	69.8	29.3	17.9	79.1	22.2	54.3	107
Cu	26.2	5.51	9.92	12.2	13.0	10.9	28.5	15.9	9.25	12.5	21.6	47.7	10.5	27.3	48.3	31.3	30.0	42.6	32.7	69.7	46.0
Zn	85.0	131	78.5	56.1	62.9	63.3	62.0	64.8	95.5	59.4	68.3	60.8	50.4	60.5	63.9	57.8	42.9	59.8	39.9	59.7	55.5
Ga	18.2	20.1	19.8	18.5	19.5	19.6	18.9	20.4	19.4	22.3	20.9	17.9	17.2	18.2	19.1	20.4	17.9	18.8	18.6	19.2	19.0
Rb	103	130	121	109	109	112	63.8	86.0	103	71.2	102	31.5	115	36.2	12.4	58.3	88.2	13.6	28.2	30.5	11.1
Sr	639	401	362	500	652	544	834	686	692	1182	699	969	398	461	1767	427	491	627	595	500	601
Y	18.3	15.8	19.3	15.5	16.4	16.0	16.4	16.6	16.0	20.1	17.4	18.7	20.7	16.1	16.9	22.3	21.2	17.3	11.7	16.6	16.8
Zr	147	142	159	149	155	162	129	172	142	230	169	128	227	129	87.4	142	210	124	136	109	109
Nb	12.3	14.0	14.0	12.3	14.4	13.1	8.48	14.8	11.2	13.2	14.4	7.68	15.3	5.74	5.62	12.0	13.2	8.43	4.73	6.33	5.91
Cs	4.96	2.88	19.8	5.55	6.43	4.98	4.12	3.33	6.85	3.27	7.32	1.38	5.16	1.85	0.59	2.72	3.69	0.46	1.20	2.40	0.42
Ba	851	537	577	495	505	534	297	595	465	425	551	253	459	235	612	257	285	134	159	208	124
La	26.7	25.9	35.7	27.9	31.6	29.9	22.3	32.5	26.8	43.7	32.7	15.6	28.5	14.5	10.8	22.4	24.2	16.0	13.0	13.1	13.0
Ce	51.8	51.6	70.7	56.5	63.9	60.6	48.1	66.3	54.2	94.7	67.6	34.4	58.1	30.9	24.3	46.2	51.2	34.6	26.1	28.4	28.6
Pr	5.61	5.74	8.31	6.35	7.11	6.82	5.71	7.44	6.18	11.2	7.64	4.16	6.30	3.69	3.05	5.50	5.98	4.42	3.12	3.67	3.70
Nd	20.7	21.2	31.4	23.7	26.3	25.3	22.2	28.0	23.0	41.3	28.8	16.9	22.5	14.9	13.0	21.0	22.0	17.5	12.0	14.9	15.1
Sm	3.66	3.81	5.70	4.15	4.64	4.55	4.09	4.86	4.09	6.39	5.07	3.54	3.97	3.01	3.00	4.51	4.42	3.70	2.46	3.33	3.30
Eu	0.94	0.97	1.28	1.02	1.11	1.06	1.06	1.18	1.00	1.60	1.23	1.02	0.96	0.89	0.95	1.24	0.98	1.15	0.81	1.03	1.06
Gd	3.27	3.15	4.56	3.39	3.62	3.50	3.42	3.86	3.39	4.83	4.01	3.44	3.48	2.90	2.98	4.28	3.94	3.41	2.28	3.20	3.16
Tb	0.50	0.47	0.65	0.49	0.53	0.51	0.51	0.54	0.49	0.66	0.58	0.51	0.54	0.45	0.46	0.66	0.61	0.52	0.34	0.49	0.49
Dy	2.97	2.71	3.42	2.68	2.89	2.73	2.82	2.94	2.68	3.55	3.07	3.20	3.26	2.67	2.90	3.96	3.64	3.03	2.05	2.88	2.95
Ho	0.63	0.56	0.69	0.55	0.57	0.55	0.59	0.58	0.55	0.71	0.61	0.69	0.70	0.56	0.62	0.84	0.76	0.65	0.42	0.59	0.62

AGU Geochemistry, Geophysics, Geosystems

10.1002/2014GC005262

Table 1. (Continued)

	Mirabad		Taftan									Bazman									
Sample	10–22	10–23	10–24	10–25	10–26	10–27	10–28	10–29	10–30	10–31	10–32	10–34	10–36	10–37	10–42	10–45	10–46	10–47	10–48	10–49	10–50
Er	1.82	1.54	1.82	1.50	1.57	1.49	1.61	1.54	1.52	1.95	1.69	1.90	2.01	1.53	1.69	2.32	2.15	1.77	1.15	1.62	1.72
Tm	0.28	0.23	0.26	0.21	0.23	0.21	0.24	0.23	0.22	0.28	0.24	0.27	0.32	0.24	0.25	0.35	0.33	0.26	0.18	0.24	0.25
Yb	1.90	1.52	1.68	1.41	1.47	1.37	1.47	1.44	1.46	1.77	1.49	1.77	2.12	1.47	1.55	2.26	2.18	1.73	1.17	1.59	1.60
Lu	0.30	0.25	0.26	0.22	0.23	0.20	0.23	0.23	0.24	0.27	0.24	0.27	0.34	0.23	0.24	0.33	0.33	0.24	0.19	0.24	0.25
Hf	3.73	3.58	3.79	3.54	3.80	3.90	3.28	4.02	3.47	5.68	3.93	2.96	5.25	2.93	2.13	3.53	5.14	2.92	3.11	2.69	2.57
Ta	0.87	1.06	0.95	0.84	1.08	0.91	0.58	0.97	0.79	0.83	0.92	0.45	1.09	0.36	0.29	0.75	0.88	0.45	0.33	0.41	0.30
Pb	128	31.8	15.9	12.0	12.7	12.6	7.70	13.2	11.6	8.57	12.2	5.97	12.0	6.35	11.5	8.11	5.10	2.81	5.23	5.65	3.57
Th	10.4	10.8	12.0	10.3	12.6	11.2	7.42	10.5	9.96	10.6	10.5	3.84	11.6	2.49	1.84	5.28	9.73	2.02	2.55	2.39	1.65
U	3.03	2.36	2.74	2.44	2.73	2.71	1.75	2.27	2.35	2.28	2.33	1.46	2.98	0.70	0.95	1.15	2.30	0.46	1.02	0.87	0.38
Isotopic Ratios																					
$^{87}Sr/^{86}Sr$	0.707638	0.708359	0.706760	0.706478	0.706280	0.706479		0.706363		0.704359		0.706507	0.705945				0.706026	0.703891			0.704084
$\pm 2\sigma_m$ [c]	0.000006	0.000007	0.000015	0.000006	0.000005	0.000005		0.000009		0.000009		0.000007	0.000009				0.000006	0.000019			0.000006
$^{143}Nd/^{144}Nd$	0.512405	0.512329	0.512413	0.512470	0.512486	0.512467		0.512476		0.512777		0.512678	0.512631				0.512697	0.512824			0.512817
$\pm 2\sigma_m$ [c]	0.000004	0.000002	0.000003	0.000003	0.000002	0.000003		0.000003		0.000003		0.000003	0.000007				0.000001	0.000004			0.000004

[a]Total iron as Fe_2O_3.
[b]Mg# = [molar 100 x Mg/(Mg + Fe^{2+})], assuming 10% of total iron oxide is ferric.
[c]The 2σ values are the mean standard deviations of the measurements.

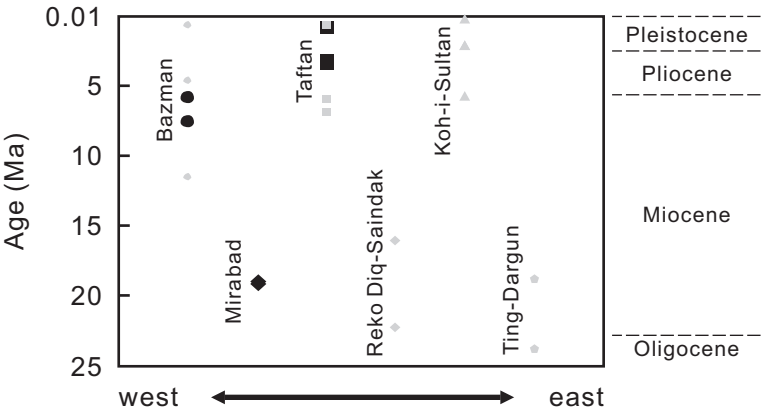

Figure 9. Magmatic ages of the Makran arc rocks. Published data are after *Conrad et al.* [1981] (K/Ar; Bazman), *Biabangard and Moradian* [2008] (K/Ar; Taftan), *Perelló* [2008] (K/Ar and $^{39}Ar/^{40}Ar$; Ting-Dargun), and *Richards et al.* [2012] ($^{39}Ar/^{40}Ar$; Koh-i-Sultan and Reko Diq-Saindak).

Fe_2O_3 (~3.3–8.1 wt %), MgO (~0.66–6.73 wt %), CaO (~3.3–11.7 wt %), and Cr (~28–187 ppm; Figures 6a–6e and 6g), and positively with K_2O (~0.84–3.0 wt %), Rb (~14–115 ppm), and La (~11–28 ppm; Figures 6h and 6i). No systematic trend exists between Na_2O and SiO_2 (Figure 6f). As shown in Figure 7c, an orogenic signature is apparent in the primitive mantle-normalized trace element diagram, and samples 10–36 and 10–46 exhibit slight positive Zr-Hf anomalies, a feature absent in the rest majority of samples. Compared with our data, samples obtained by *Saadat and Stern* [2011] for the Bazman monogenetic parasitic cones extend to low SiO_2 compositions down to ~45 wt %, but the trace element patterns for their samples and our samples largely overlap (Figure 7c). The Bazman samples have $^{87}Sr/^{86}Sr$ ranging from 0.7039 to 0.7065 and $^{143}Nd/^{144}Nd$ from 0.5126 to 0.5128, extending from ratios similar to the Bulk Silicate Earth to depleted isotopic compositions (Figure 8 and Table 1).

5. Discussion

5.1. The Makran as a Neogene-Quaternary Subduction System

One important finding derived from this study is that the Makran arc magmatism might have started considerably earlier than generally appreciated. As summarized above, existing age data for the arc rocks range from the Late Miocene to Quaternary. Our new data show that the Mirabad pluton in the vicinity of the Taftan volcano formed at ~19 Ma, which predated the Taftan volcano for at least 12 Myr (Figure 9). Although ~19 Ma ages are unknown from large eruptive centers of the arc like Bazman and Koh-i-Sultan, there are Late Oligocene-Early Miocene magmatic ages reported in the Pakistan Makran, including Reko Diq-Saindak (~16 and ~22 Ma) [*Perelló*, 2008; *Richards et al.*, 2012] and Ting-Dargun (~19 and ~24 Ma) [*Perelló*, 2008] (Figure 9). It is therefore very likely that the Taftan region and some regions in the Pakistan Makran was magmatically active by the Early Miocene and it is important whether this pulse of magmatism is related to the Makran arc or to the Zahedan-Shah Kuh belt composed of Oligocene-Miocene plutons (Figure 1a). Our data show that rocks from the Mirabad pluton and the Taftan volcano are geochemically similar, consistent with a common petrogenetic relationship. In detail, the time-integrated enrichment in Sr-Nd isotopes is a diagnostic feature as the majority of Cenozoic magmatic rocks in Iran are characterized by depleted Sr-Nd isotopic compositions [*Omrani et al.*, 2008; *Ahmadian et al.*, 2009; *Aghazadeh et al.*, 2010; *Allen et al.*, 2013; *Pang et al.*, 2013a] characteristic of juvenile, or oceanic-type, terrane. The ~32 Ma Zahedan pluton shows depletions in Y and heavy rare earth elements, and depleted to Bulk Silicate Earth-like Sr-Nd isotopic compositions [*Sadeghian et al.*, 2005; *Zarrinkoub et al.*, unpublished manuscript, 2014], features that compare differently to the Mirabad and Taftan samples. It is thus more likely, from a geochemical perspective, that the Mirabad pluton represents the root of an Early Miocene volcano that is compositionally similar to the Taftan volcano. Finally, the locality Ting-Dargun where ~19 and ~24 Ma andesitic rocks were documented is located far from the Zahedan-Shah Kuh belt, but lying along the chain of the Makran arc volcanoes (Figure 1a). We thus believe that the Makran arc did consist of a magmatic pulse in the Early Miocene and arc magmatism presumably started by that time.

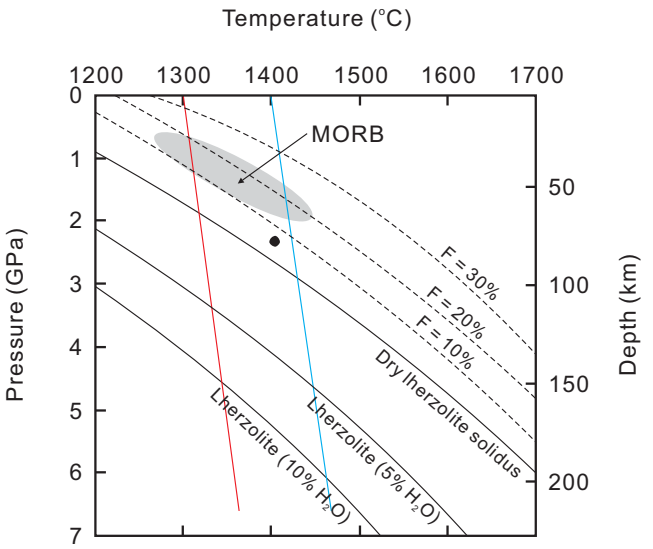

Figure 10. The estimated temperature and pressure of a basaltic sample from the Makran arc, southeastern Iran, using the thermobarometers established by *Lee et al.* [2009] (see text for discussion). The sample used is B-21 collected from the Bazman region by *Saadat and Stern* [2011]. The red and blue lines denote solid mantle adiabats with mantle potential temperatures of 1300°C and 1400°C, respectively. The MORB field is after *Lee et al.* [2009]. Lherzolite solidi for various H_2O contents and melt fraction isopleths are after *Katz et al.* [2003].

5.2. Petrogenetic Constraints

All studied samples do not meet the criteria for primitive magmas in equilibrium with mantle peridotites, i.e., >400–500 ppm Ni, >1000 ppm Cr, and Mg# > 70 [*Wilson*, 1989]. However, the following geochemical features point to contribution from the mantle in magma genesis: (i) the basaltic and andesitic compositions (<56 wt % SiO_2) of some Bazman and Taftan samples (Figure 5a), (ii) the moderate to high concentrations of Ni (38–171 ppm except one outlying datum), Cr (90–240 ppm except one outlying datum), and Mg# (51–65) in these samples, and (iii) the low $^{143}Nd/^{144}Nd$ (0.5127–0.5128) for these samples compared to the Bulk Silicate Earth, indicating time-integrated LREE depletion characteristic of mantle-derived magmas. The above features are consistent with the widely accepted hypothesis that arc magmas originate in the subarc upper mantle [*Gill*, 1981; *Thorpe*, 1982; *Pearce and Peate*, 1995]. *Lee et al.* [2009] presented new thermobarometers based on Si and Mg contents of basaltic magmas to estimate the temperature and pressure (P-T) of magma generation. Using the Excel spreadsheet developed by these authors for fractionation correction and P-T estimation, we obtain ~1400°C and ~2.3 GPa for a basaltic sample in the vicinity of the Bazman volcano (Figure 10). It is the only available analysis in the Makran arc having MgO high enough (>8.5 wt %) for estimation on anhydrous basis. Because the qualitative effect of H_2O addition is a shift to lower temperature and higher pressure [see *Lee et al.*, 2009], the estimated pressure of ~2.3 GPa can be considered a minimum pressure of magma generation, corresponding to a depth of ~76 km in the subarc upper mantle.

Samples with >3 wt % MgO (on a volatile-free basis), a subset which should be less strongly affected by magma differentiation are screened to examine the features of the mantle source. Because of limited fluid mobility and different relative incompatibilities, the elements Nb and Yb are ideal to examine the degree of enrichment (or depletion) of the magma source. The Nb/Yb of this subset of samples is from ~3.6 to ~9.7, a range lying between values of average enriched mid-ocean ridge basalt (E-MORB; ~3.5) and oceanic island basalts (OIB; ~22) [see *Sun and McDonough*, 1989]. This indicates that the mantle source is enriched in the more incompatible trace elements (e.g., Nb) or the degree of melting is low, or a combination of both. However, the calc-alkaline character of the studied rocks is consistent with normal degrees of mantle melting in arc settings (i.e., ~5–15%) and the alternative possibility of magma derivation from an enriched mantle source appears more plausible. Similar arguments apply for elemental ratios Zr/Nb (~12–22), Zr/Y (~5.2–11), and Nb/Y (~0.33–0.83) that compare closely to E-MORB-OIB ranges [see *Sun and McDonough*, 1989]. We then plot Ba/Yb, Th/Yb, La/Yb, and Pb/Yb against Nb/Yb to investigate the behavior of LILE, LREE, Th, and Pb. As shown in Figure 11, the data plot above the mantle array indicative of the nonconservative behavior of these elements characteristic of arc magmas [*Pearce and Peate*, 1995]. Also, the subparallel trends defined by these data to the mantle array can be readily explained by constant addition of a subduction component to the mantle source followed by dynamic melting [*Pearce et al.*, 1995]. *Plank* [2005] developed Th/La as a rigorous proxy for sediment recycling in subduction zones. The study demonstrated that arc magmas inherit Th/La from subducted sediments and high Th/La is not generated during subduction. Relatively high Th/La of the studied samples can be interpreted in a similar manner by mixing between an enriched mantle end-member like E-MORB and subducted sediments with high and variable Th/La (Figure 12a). No systematic relations exist between the sediment proxy Th/La and Ba/Th (Figure 12b), a

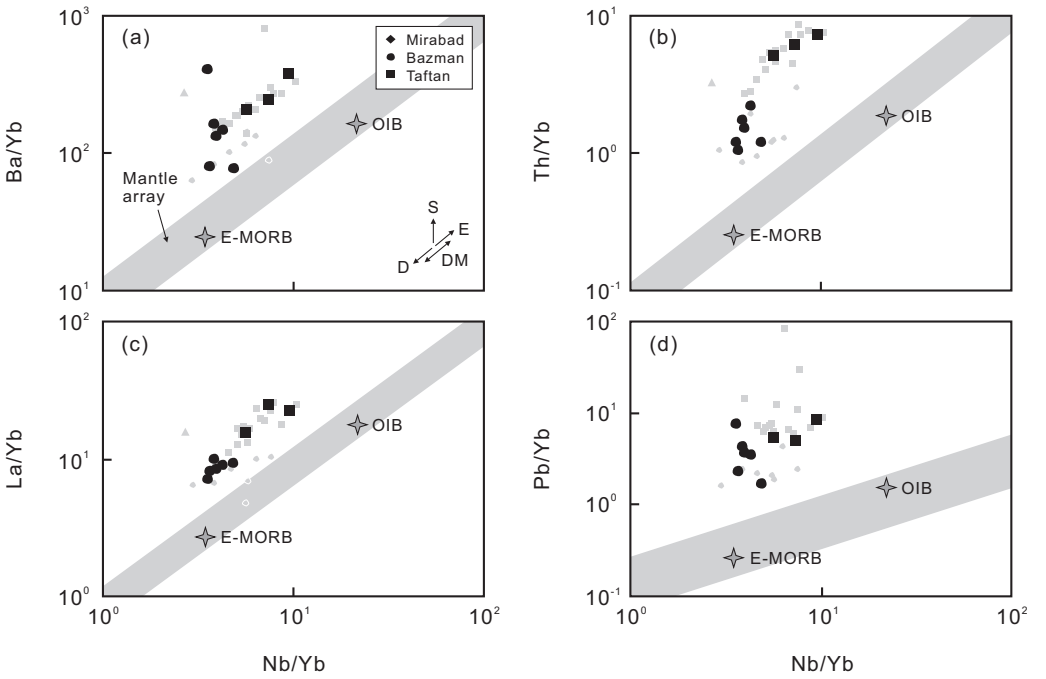

Figure 11. Yb-normalized trace element variation diagrams [after *Pearce and Peate*, 1995]. The *x* axes denote Nb/Yb and *y* axes denote (a) Ba/Yb, (b) Th/Yb, (c) La/Yb, and (d) Pb/Yb. Published geochemical data of MORB and OIB used to construct the mantle array are after *Mahoney et al*. [1998], *Doucet et al*. [2004], *Nohda et al*. [2005], *Murton et al*. [2005], and *Zhang et al*. [2005]. Only the basaltic and relatively primitive andesitic samples (>3 wt % MgO) are plotted. Vectors for subduction addition (S), mantle enrichment (E) and depletion (D), and dynamic melting (DM) are shown for reference.

proxy for shallow subduction component, or Ce/Pb (Figure 12c), a measure of the extent of the positive Pb anomaly. As shown in these diagrams, some samples having Ba/Th higher than E-MORB and Ce/Pb lower than the upper continental crust most likely reflect enrichment of LILE and Pb by hydrous fluid. In addition, the Th/La of the relatively primitive samples clusters over a range of $^{143}Nd/^{144}Nd$ (Figure 12d), indicating that the isotopic variations are not primarily controlled by sediment melt addition (see later discussion).

As noted above, the studied rocks have compositions more evolved than any putative primitive magmas such that differentiation by fractional crystallization, with or without concomitant crustal contamination, can be expected. As shown in Figure 13 (inset), the tendency for samples with higher MgO to have lower $^{87}Sr/^{86}Sr$, and vice versa, is consistent with the process of combined assimilation and fractional crystallization. However, the data cluster in a diagram of Sr versus $^{87}Sr/^{86}Sr$ (Figure 13), an observation at odds with the positive correlation between Sr and its isotopic composition in the "Bazman arc rocks" noted by *Ahmadian et al*. [2009]. The rocks referred to by these authors are, however, belong to the Bazman intrusive complex recently dated using zircon U-Pb method at the Late Cretaceous [*Chiu et al*., 2013] such that these rocks might not be directly comparable to the much younger Bazman volcano. The spread of data in Figure 13 cannot be explained by any simple classical assimilation-fractional crystallization (AFC) models, and we here attempt to model the data using the more robust, energy-constrained assimilation-fractional crystallization (EC-AFC) model established by *Bohrson and Spera* [2001] and *Spera and Bohrson* [2001]. The parameters are given in Table 2, including an initial magma with 500 ppm Sr and $^{87}Sr/^{86}Sr$ of ~0.7039, a felsic assimilant with 156 ppm Sr and $^{87}Sr/^{86}Sr$ of 0.7157 and a mafic assimilant with 300 ppm Sr and $^{87}Sr/^{86}Sr$ of 0.7097. The results show that the elemental and isotopic variations of Sr can be modeled by variable bulk distribution coefficients (D) for Sr in magma and assimilant from neutral ($D_m = D_a = 1$) to moderately incompatible ($D_m = D_a = 0.4$) (Figure 13), and the nature of the assimilant appears to be of secondary importance. The incompatible behavior of Sr might reflect a feldspar-poor assimilant and/or limited involvement of feldspar during differentiation [see *Guo et al*., 2006]. A caveat for the above model is that D is treated constant for each trajectory—the actual behavior of Sr in magmas ought to be more complicated, possibly involving a change from incompatible to compatible at the point of plagioclase saturation, a case

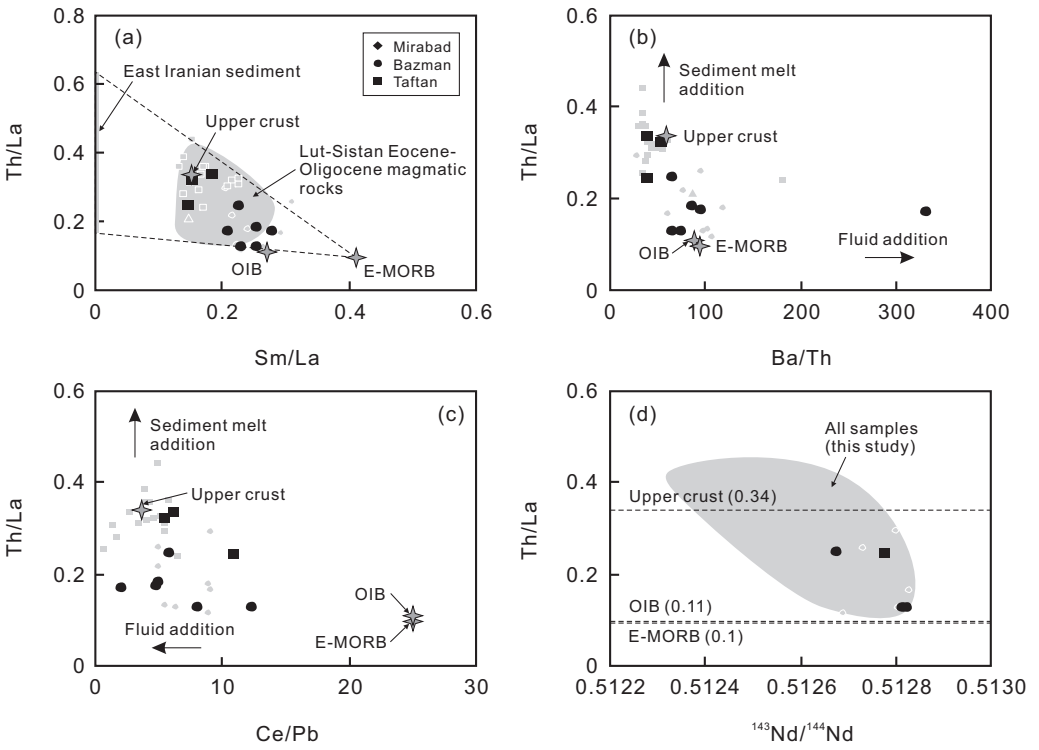

Figure 12. Binary diagrams illustrating the role of sediment partial melt and hydrous fluid in the genesis of the Makran arc rocks. (a) Th/La versus Sm/La. The shaded region denoting the compositional variations of Eocene-Oligocene magmatic rocks in the Lut-Sistan region, eastern Iran is after *Pang et al.* [2013a]. (b) Th/La versus Ba/Th. (c) Th/La versus Ce/Pb. (d) Th/La versus $^{143}Nd/^{144}Nd$. The shaded region denotes the compositional variations of all studied rocks. Only the basaltic and relatively primitive andesitic samples (>3 wt % MgO) are plotted. E-MORB and OIB values are after *Sun and McDonough* [1989], and the values for average upper continental crust are after *Rudnick and Gao* [2003].

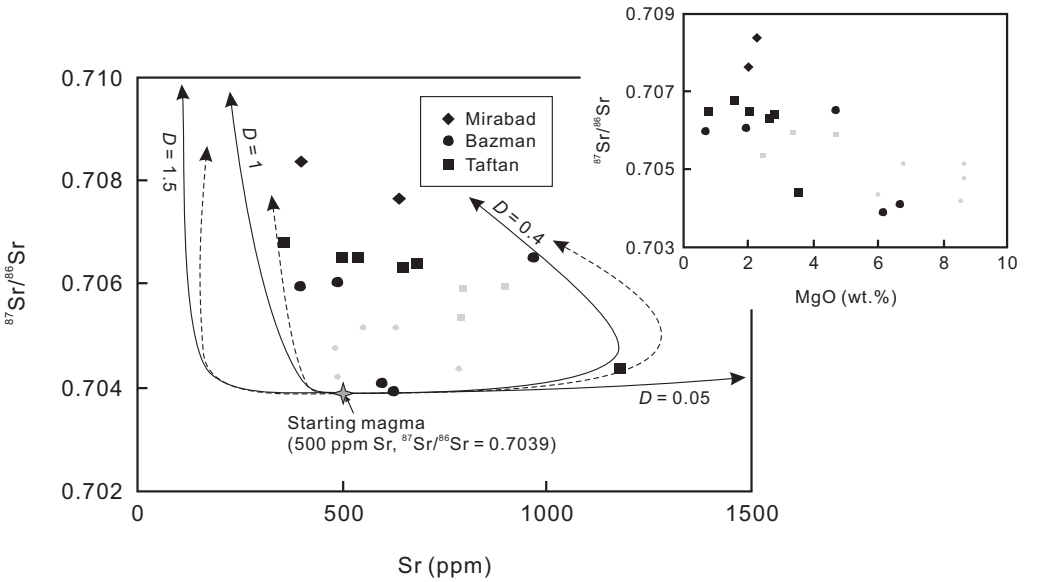

Figure 13. A plot of $^{87}Sr/^{86}Sr$ versus Sr illustrating the results of the EC-AFC modeling (see text for discussion and Table 2 for modeling parameters). Solid arrows denote AFC trajectories for the felsic assimilant, and dashed arrows denote such trajectories for the mafic assimilant. D = Sr distribution coefficient for magma and assimilant. Inset shows a plot of $^{87}Sr/^{86}Sr$ versus MgO.

Table 2. Parameters Used for EC-AFC Modeling

Thermal Parameters			
Magma liquidus temperature ($T_{l,m}$, °C)	1300	Crystallization enthalpy (Δh_{cry}, J kg^{-1})	396,000
Magma initial temperature (T_m°, °C)	1300	Isobaric specific heat of magma ($C_{p,m}$, J kg^{-1} K^{-1})	1484
Assimilant liquidus temperature ($T_{l,a}$, °C)	1150	Fusion enthalpy (Δh_{fus}, J kg^{-1})	270,000
Assimilant initial temperature (T_a°, °C)	600	Isobaric specific heat of assimilant ($C_{p,a}$, J kg^{-1} K^{-1})	1370
Solidus temperature (T_s, °C)	900		
Equilibration temperature (T_{eq}, °C)	1000		

Compositional Parameters	Felsic Assimilant[c]	Mafic Assimilant[d]
Magma initial Sr concentration (C_m°, ppm)[a]	500	500
Magma $^{87}Sr/^{86}Sr$ (ε_m)[a]	0.7039	0.7039
Magma bulk distribution coefficient for Sr (D_m)[b]	(0.05, 0.4, 1, 1.5)	(0.05, 0.4, 1, 1.5)
Assimilant initial Sr concentration (C_a°, ppm)	156	300
Assimilant $^{87}Sr/^{86}Sr$ (ε_a)	0.7157	0.7097
Assimilant bulk distribution coefficient for Sr (D_a)[b]	(0.05, 0.4, 1, 1.5)	(0.05, 0.4, 1, 1.5)

[a] C_m° and ε_m are inferred from samples with relatively high MgO and low $^{87}Sr/^{86}Sr$ [*Saadat and Stern*, 2011, this study].
[b] D_m and D_a are chosen as if Sr behaves as highly incompatible to slightly compatible.
[c] C_a° and ε_a for the felsic assimilant is taken from a meta-granite (sample IRK-GR1) from the Khoy metamorphic complex [*Azizi et al.*, 2011].
[d] C_a° and ε_a for the mafic assimilant is taken from a meta-basite (sample IRK-AM2) from the Khoy metamorphic complex [*Azizi et al.*, 2011].

difficult to be modeled by EC-AFC. However, it is apparent that the incompatible behavior of Sr is required to explain samples with >500 ppm Sr and $^{87}Sr/^{86}Sr > 0.7039$ for the assimilants examined.

5.3. A Three-Component Model for Magma Genesis

The petrogenetic constraints placed in the earlier section allow the establishment of a generalized model for magma genesis in the Makran arc. As described and explained below, the model consists of three components that are essential to explain the geochemical variations of the studied rocks.

A depleted mantle component. The component is signified by the unradiogenic Sr and radiogenic Nd isotopic compositions, indicating time-integrated LILE and LREE depletion compared to the Bulk Silicate Earth. The component likely represents the subarc mantle wedge that underwent melt extraction long enough to impart a depleted signal with respect to Sr-Nd isotopes. At Makran, this component is the most obvious in the basaltic samples from the Bazman volcano.

A trace element-rich component. The component is marked by enrichments in all incompatible trace elements and is responsible for imparting an orogenic geochemical signature to the mantle source. Although its Rb/Sr is higher and Sm/Nd lower than the Bulk Silicate Earth, the component does not reside in the lithosphere long enough to evolve to enriched Sr-Nd isotopic compositions. The component likely represents partial melts of subducted sediments and/or slab-derived hydrous fluid. At Makran, this component is hidden in the relatively primitive samples showing orogenic signatures and depleted Sr-Nd isotopic compositions from the Bazman and Taftan volcanoes.

An isotopically enriched component. The component is characterized by radiogenic Sr and unradiogenic Nd isotopic compositions, suggesting time-integrated LILE and LREE enrichment compared to the Bulk Silicate Earth. The component likely represents the continental crust whose elements were extracted from the mantle long enough for the Sr-Nd isotopes to evolve to enriched compositions. In theory, it should also exhibit an orogenic signature as component 2 [see *Rudnick and Gao*, 2003]. At Makran, this component is the strongest in the Mirabad and Taftan samples.

Although it could be argued that components 2 and 3 can be taken together to represent subducted sediments whose source rocks reside in the crust long enough to acquire enriched isotopic signatures, we do not prefer such an interpretation for the Makran arc because: (i) no negative trend is observed between Th/La and $^{143}Nd/^{144}Nd$ for the relatively primitive samples (Figure 12d), as would be expected if the variable addition of old sediment melt to the mantle source happened, (ii) these samples are enriched in terms of trace element concentrations coupled with depleted Sr-Nd isotopic compositions, indicating that the enrichment was a relatively recent event without significant involvement of old sediments in the petrogenesis, and (iii) the Sr-Nd isotopic compositions of the studied samples are not consistent with binary mixing between depleted MORB mantle [*Workman and Hart*, 2005] and global subducting sediment (GLOSS) [*Plank and Langmuir*, 1998] or Tethyan flysch [*Prelevic et al.*, 2008] (Figure 8). We thus consider that components 2

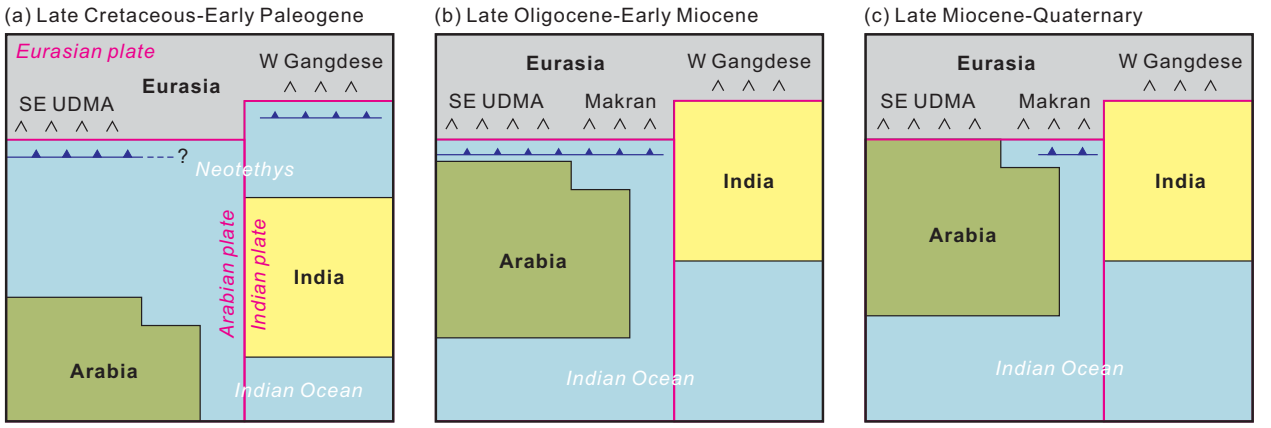

Figure 14. Schematic diagrams illustrating the tectonic evolution of the Makran and surrounding regions (not to scale). (a) Late Cretaceous to Early Paleogene: northward subduction of the Neotethys beneath southern Eurasia generated the UDMA and the Gangdese arcs in association with the dominantly northward drift of India and Arabia. (b) Late Oligocene-Early Miocene: India and Eurasia collided to each other while the Arabia-Eurasia collision had started further to the north in a diachronous manner, leaving a narrow ocean tract in the southern part of the collision zone. Northward subduction of the Arabian plate propagated eastward generating the Makran arc. (c) Late Miocene-Quaternary: diachronous collision between Arabia and Eurasia completed and the Makran arc magmatism continued due to the northward subduction of the oceanic portion of the Arabian plate.

and 3 have no genetic relation to each other in the Makran arc. The model presented above has the advantage to explain the lack of coupled enrichment in terms of trace elements and radiogenic isotopes, and might be applicable to some other arc systems, particularly continental arcs.

5.4. Tectonic Implications

Our results shed new lights on the geodynamic evolution of the Makran presented by *McCall* [1997, 2002]. He noted that there were probably two coexisting subduction zones in the Makran during the Paleogene, one at which is now the southeastern UDMA and another resulted in a plutonic belt from Zahedan to Shah-Kuh running subparallel to it (Figure 1a). It was proposed that magmatic activity of the latter ceased toward the end of the Oligocene whereas the former shifted out in the Gulf of Oman at the Early Pliocene, a change accompanied by uplift and subsequent formation of the Makran arc. However, the initiation of the Makran arc magmatism at the Early Miocene, as discussed earlier based on our new data, implies that the Makran subduction likely began at pre-Miocene times. Recent zircon U-Pb dating results by *Chiu et al.* [2013] confirm that magmatic activity of the southeastern UDMA continued to the latest Pliocene. In view of the above, a likely scenario is that the Neotethyan subduction zone that generated the UDMA propagated from the northwest to southeast in the Gulf of Oman at pre-Miocene times and northward subduction since then produced the Makran arc (Figures 14a and 14b). A sudden jump of the subduction front at the Early Pliocene, as argued by *McCall* [1997, 2002], probably did not happen.

Based on available data and observations, we propose that the Makran represents a window of continental collision between the India-Eurasia collision zone to the east and the Arabia-Eurasia collision zone to the west (see Figure 14 for details). It is part of the southern margin of Eurasia where remnant oceanic lithosphere of the Neotethys, as shown by heat flow data by *Hutchison et al.* [1981], has been destroyed in a subduction zone since the Early Miocene. At that time, a large part of Neotethys had been consumed in subduction zones along what are now the Indus-Yarlung suture to the east and the Bitlis-Zagros suture to the west. Prior to Miocene, it is either that subduction was inactive along this segment of the continental margin or that it did happened but left no magmatic record for some unknown reasons. An analogy can be drawn with the eastern Mediterranean that is also underlain by remnant Neotethyan oceanic lithosphere [*Garfunkel*, 2004, and references therein; *Müller et al.*, 2008]. A major difference is that the Mediterranean Sea will be closed in the future when Africa and Eurasia finally converge, whereas oceanic lithosphere of the Indian Ocean will continue to subduct beneath the Makran arc until the arrival of a continental block at the subduction zone.

6. Concluding Remarks

The important results of this study are summarized below:

1. Magmatic activity of the Makran arc, previously considered to be active from the Late Miocene to Quaternary, might have actually commenced by the Early Miocene. The argument is based on the ~19 Ma Mirabad pluton that is geochemically similar to the Taftan volcano.

2. The compositions of the Makran arc magmas are consistent with derivation from subduction-modified upper mantle and subsequent modification by assimilation-fractional crystallization.
3. A petrogenetic model involving three components—a depleted mantle component, a trace element-rich component, and an isotopically enriched component—can explain the geochemical and Sr-Nd isotopic variations of the studied rocks. They are taken to represent the subarc upper mantle, sediment melt, and/or slab-derived hydrous fluid, and the continental crust, respectively.
4. The subduction zone generating the Makran arc might have been propagated from the one resulted in the UDMA to the northwest. The Makran represents a window of continental collision between the India-Eurasia collision zone to the east and the Arabia-Eurasia collision zone to the west.

Acknowledgments
The data for this paper are available in Table 1 and the tables in supporting information, and can be released upon written request to the corresponding author. We thank Chiu-Hong Chu, Hao-Yang Lee, Te-Hsien Lin, Hsin-Yi Chang, and Yu-Chen Chen for laboratory assistance. Reviews by Jonathan Miller and an anonymous reviewer led to substantial improvement in clarity of the final manuscript. This study was performed jointly by University of Birjand and National Taiwan University, and gained financial support from a project (102PFA0100650) awarded to S.L.C. by the National Science Council, Taiwan.

References

Agard, P., J. Omrani, L. Jolivet, H. Whitechurch, B. Vrielynck, W. Spakman, P. Monié, B. Meyer, and R. Wortel (2011), Zagros orogeny: A subduction-dominated process, *Geol. Mag.*, *148*, 692–725.
Aghazadeh, M., A. Castro, N. R. Orman, M. H. Emami, H. Moinvaziri, and Z. Badrzadeh (2010), The gabbro (shoshonitic)-monzonite-granodiorite association of Khankandi pluton, Alborz Mountains, NW Iran, *J. Asian Earth Sci.*, *38*, 199–219.
Ahmadian, J., M. Haschke, I. McDonald, M. Regelous, M. RezaGhorbani, M. H. Emami, and M. Murata (2009), High magmatic flux during Alpine-Himalayan collision: Constraints from the Kal-e-Kafı complex, central Iran, *Geol. Soc. Am. Bull.*, *121*, 857–868.
Alavi, M. (1994), Tectonics of the Zagros orogenic belt of Iran: New data and interpretations, *Tectonophysics*, *229*, 211–238.
Alavi, M., H. Vaziri, K. Seyed-Emami, and Y. Lasemi (1997), The Triassic and associated rocks of the Nakhlak and Aghdarband areas in central and northeastern Iran as remnants of the southern Turanian active continental margin, *Geol. Soc. Am. Bull.*, *109*, 1563–1575.
Allen, M. B., and H. A. Armstrong (2008), Arabia-Eurasia collision and the forcing of mid-Cenozoic global cooling, *Palaeogeogr. Palaeoclimatol. Palaeoecol.*, *265*, 52–58.
Allen, M. B., M. Kheirkhah, I. Neill, M. H. Emami, and C. L. McLeod (2013), Generation of arc and within-plate chemical signatures in collision zone magmatism: Quaternary lavas from Kurdistan Province, Iran, *J. Petrol.*, *54*, 887–911.
Angiboust, S., P. Agard, J. C. M. De Hoog, J. Omrani, and A. Plunder (2013), Insights on deep, accretionary subduction processes from the Sistan ophiolitic "melange" (Eastern Iran), *Lithos*, *156–159*, 139–158.
Azizi, H., S.-L. Chung, T. Tanaka, and Y. Asahara (2011), Isotopic dating of the Khoy metamorphic complex (KMC), northwestern Iran: A significant revision of the formation age and magma source, *Precambrian Res.*, *185*, 87–94.
Ballato, P., C. E. Uba, A. Landgraf, M. R. Strecker, M. Sudo, D. F. Stockli, A. Friedrich, and S. H. Tabatabaei (2011), Arabia-Eurasia continental collision: Insights from late Tertiary foreland-basin evolution in the Alborz Mountains, northern Iran, *Geol. Soc. Am. Bull.*, *123*, 106–131.
Berberian, M., and G. C. P. King (1981), Towards a paleogeography and tectonic evolution of Iran, *Can. J. Earth Sci.*, *18*, 210–265.
Biabangard, H., and A. Moradian (2008), Geology and geochemical evaluation of Taftan Volcano, Sistan and Baluchestan Province, southeast of Iran, *Chin. J. Geochem.*, *27*, 356–369.
Bohrson, W. A., and F. J. Spera (2001), Energy-constrained open-system magmatic processes II: Application of energy-constrained assimilation-fractional crystallization (EC-AFC) model to magmatic systems, *J. Petrol.*, *42*, 1019–1041.
Byrne, D. E., L. R. Sykes, and D. M. Davis (1992), Great thrust earthquakes and aseismic slip along the plate boundary of the Makran subduction zone, *J. Geophys. Res.*, *97*, 449–478.
Camp, V. E., and R. J. Griffis (1982), Character, genesis and tectonic setting of igneous rocks in the Sistan suture zone, eastern Iran, *Lithos*, *15*, 221–239.
Chiu, H.-Y., S.-L. Chung, M. H. Zarrinkoub, S. S. Mohammadi, M. H. Khatib, and Y. Iizuka (2013), Zircon U-Pb age constraints from Iran on the magmatic evolution related to Neotethyan subduction and Zagros orogeny, *Lithos*, *162–163*, 70–87.
Conrad, G., R. Montigny, R. Thuizat, and M. Westphal (1981), Tertiary and Quaternary geodynamics of southern Lut (Iran) as deduced from palaeomagnetic, isotopic and structural data, *Tectonophysics*, *75*, 11–17.
Davidson, J., J. Hassanzadeh, R. Berzins, D. F. Stockli, B. Bashukooh, B. Turrin, and A. Pandamouz (2004), The geology of the Damavand volcano, Alborz Mountains, northern Iran, *Geol. Soc. Am. Bull.*, *116*, 16–29.
Dewey, J. F., W. C. Pitman III, W. B. F. Ryan, and J. Bonnin (1973), Plate tectonics and the evolution of the Alpine system, *Geol. Soc. Am. Bull.*, *84*, 3137–3180.
Doucet, S., D. Weis, J. S. Scoates, V. Debaille, and A. Giret (2004), Geochemical and Hf-Pb-Sr-Nd isotopic constraints on the origin of the Amsterdam-St. Paul (Indian Ocean) hotspot basalts, *Earth Planet. Sci. Lett.*, *218*, 179–195.
Farhoudi, G., and D. E. Karig (1977), Makran of Iran and Pakistan as an active arc system, *Geology*, *5*, 664–668.
Garfunkel, Z. (2004), Origin of the Eastern Mediterranean basin: A reevaluation, *Tectonophysics*, *391*, 11–34.
Garzanti, E., S. Critelli, and R. V. Ingersoll (1996), Paleogeographic and paleotectonic evolution of the Himalayan Range as reflected by detrital modes of Tertiary sandstones and modern sands (Indus transect, India and Pakistan), *Geol. Soc. Am. Bull.*, *108*, 631–642.
Ghazi, A. M., A. A. Hassanipak, J. J. Mahoney, and R. A. Duncan (2004), Geochemical characteristics, ^{40}Ar-^{39}Ar ages and original tectonic setting of the Band-e-Zeyarat/Dar Anar ophiolite, Makran accretionary prism, S.E. Iran, *Tectonophysics*, *393*, 175–196.
Gill, J. B. (1981), *Orogenic Andesites and Plate Tectonics*, Springer, Berlin.
Grando, G., and K. McClay (2007), Morphotectonics domains and structural styles in the Makran accretionary prism, offshore Iran, *Sediment. Geol.*, *196*, 157–179.
Guo, Z., M. Wilson, J. Liu, and Q. Mao (2006), Post-collisional, potassic and ultrapotassic magmatism of the northern Tibetan Plateau: Constraints on characteristics of the mantle source, geodynamic setting and uplift mechanisms, *J. Petrol.*, *47*, 1177–1220.
Hassanzadeh, J., D. F. Stockli, B. K. Horton, G. J. Axen, L. D. Stockli, M. Grove, A. K. Schmitt, and J. D. Walker (2008), U-Pb zircon geochronology of late Neoproterozoic-Early Cambrian granitoids in Iran: Implications for paleogeography, magmatism, and exhumation history of Iranian basement, *Tectonophysics*, *451*, 71–96.
Hutchison, I., K. E. Louden, R. S. White, and R. P. von Herzen (1981), Heat flow and age of the Gulf of Oman, *Earth Planet. Sci. Lett.*, *56*, 252–262.
Jahangiri, A. (2007), Post-collisional Miocene adakitic volcanism in NW Iran: Geochemical and geodynamic implications, *J. Asian Earth Sci.*, *30*, 433–447.

Jung, D., J. Keller, R. Khorasani, C. Marcks, A. Baumann, and P. Horn (1983), Petrology of the Tertiary magmatic activity in the northern Lut area, east of Iran, *Rep. 51*, pp. 285–336, Geol. Surv. of Iran, Tehran.

Katz, R. F., M. Spiegelman, and C. H. Langmuir (2003), A new parameterization of hydrous mantle melting, *Geochem. Geophys. Geosyst.*, *4*(9), 1073, doi:10.1029/2002GC000433.

Kheirkhah, M., M. B. Allen, and M. Emami (2009), Quaternary syn-collision magmatism from the Iran/Turkey borderlands, *J. Volcanol. Geotherm. Res.*, *182*, 1–12.

Kopp, C., J. Fruehn, E. R. Flueh, C. Reichert, N. Kukowski, J. Bialas, and D. Klaeschen (2000), Structure of the Makran subduction zone from wide-angle and reflection seismic data, *Tectonophysics*, *329*, 171–191.

Kukowski, N., T. Schillhorn, E. R. Flueh, and K. Huhn (2000), Newly identified strike-slip plate boundary in the northeastern Arabian Sea, *Geology*, *28*, 355–358.

Kuno, H. (1968), Differentiation of basalt magmas, in *Basalts: The Poldervaart Treatise on Rocks of Basaltic Composition*, vol. 2, edited by H. H. Hess and A. A. Poldervaart, pp. 623–688, Interscience, New York.

Lee, C.-T. A., P. Luffi, T. Plank, H. Dalton, and W. P. Leeman (2009), Constraints on the depths and temperatures of basaltic magma generation on Earth and other terrestrial planets using new thermobarometers for mafic magmas, *Earth Planet. Sci. Lett.*, *279*, 20–33.

Lustrino, M., S. Duggen, and C. L. Rosenberg (2011), The Central-Western Mediterranean: Anomalous igneous activity in an anomalous collisional tectonic setting, *Earth Sci. Rev.*, *104*, 1–40.

Mahoney, J. J., R. Frei, M. L. G. Tejada, X.-X. Mo, P. T. Leat, and T. F. Nägler (1998), Tracing the Indian Ocean mantle domain through time: Isotopic result from old West Indian, East Tethyan, and South Pacific seafloor, *J. Petrol.*, *39*, 1285–1306.

Marone, C., and C. H. Scholz (1988), The depth of seismic faulting and the upper transition from stable to unstable slip regimes, *Geophys. Res. Lett.*, *15*, 621–624.

McCall, G. J. H. (1997), The geotectonic history of the Makran and adjacent areas of southern Iran, *J. Asian Earth Sci.*, *15*, 517–531.

McCall, G. J. H. (2002), A summary of the geology of the Iranian Makran, in *The Tectonic and Climatic Evolution of the Arabian Sea Region, Geol. Soc. Spec. Publ.*, vol. 195, edited by P. D. Clift et al., pp. 147–204, Geol. Soc. Publ. House, Bath, U. K.

McQuarrie, N., J. M. Stock, C. Verdel, and B. P. Wernicke (2003), Cenozoic evolution of Neotethys and implications for the causes of plate motions, *Geophys. Res. Lett.*, *30*(20), 2036, doi:10.1029/2003GL017992.

McQuarrie, N., and D. J. J. van Hinsbergen (2013), Retrodeforming the Arabia-Eurasia collision zone: Age of collision versus magnitude of continental subduction, *Geology*, *41*, 315–318.

Mountain, G., and W. I. Prell (1990), A multiphase plate tectonic history of the southeast continental margin of Oman, in *The Geology and Tectonics of the Oman Region, Geol. Soc. Spec. Publ.*, 49, pp. 725–743.

Müller, R. D., M. Sdrolias, C. Gaina, and W. R. Roest (2008), Age, spreading rates, and spreading asymmetry of the world's ocean crust, *Geochem. Geophys. Geosyst.*, *9*, Q04006, doi:10.1029/2007GC001743.

Murton, B. J., A. G. Tindle, J. A. Milton, and D. Sauter (2005), Heterogeneity in southern Central Indian Ridge MORB: Implications for ridge-hot spot interaction, *Geochem. Geophys. Geosyst.*, *6*, Q03E20, doi:10.1029/2004GC000798.

Nohda, S., I. Kaneoka, T. Hanyu, S. Xu, and K. Uto (2005), Systematic variation of Sr-, Nd- and Pb-isotopes with time in lavas of Mauritius, Réunion hotspot, *J. Petrol.*, *46*, 505–522.

Omrani, J., P. Agard, H. Whitechurch, M. Benoit, G. Prouteau, and L. Jolivet (2008), Arc-magmatism and subduction history beneath the Zagros Mountains, Iran: A new report of adakites and geodynamic consequences, *Lithos*, *106*, 380–398.

Pang, K.-N., S.-L. Chung, M. H. Zarrinkoub, S. S. Mohammadi, H.-M. Yang, C.-H. Chu, H.-Y. Lee, and C.-H. Lo (2012), Age, geochemical characteristics and petrogenesis of Late Cenozoic intraplate alkali basalts in the Lut-Sistan region, eastern Iran, *Chem. Geol.*, *306–307*, 40–53.

Pang, K.-N., S.-L. Chung, M. H. Zarrinkoub, M. M. Khatib, S. S. Mohammadi, H.-Y. Chiu, C.-H. Chu, H.-Y. Lee, and C.-H. Lo (2013a), Eocene-oligocene post-collisional magmatism in the Lut-Sistan region, eastern Iran: Magma genesis and tectonic implications, *Lithos*, *180–181*, 234–251.

Pang, K.-N., S.-L. Chung, M. H. Zarrinkoub, Y.-C. Lin, H.-Y. Lee, C.-H. Lo, and M. M. Khatib (2013b), Iranian ultrapotassic volcanism at ~11 Ma signifies the initiation of post-collisional magmatism in the Arabia-Eurasia collision zone, *Terra Nova*, *25*, 405–413.

Pearce, J. A., and D. W. Peate (1995), Tectonic implications of the composition of volcanic arc magmas, *Annu. Rev. Earth Planet. Sci.*, *23*, 251–285.

Pearce, J. A., P. E. Baker, P. K. Harvey, and I. W. Luff (1995), Geochemical evidence for subduction fluxes, mantle melting and fractional crystallization beneath the South Sandwich island arc, *J. Petrol.*, *36*, 1073–1109.

Peccerillo, A., and S. R. Taylor (1976), Geochemistry of Eocene calc-alkaline volcanic rocks from the Kastamonu area, Northern Turkey, *Contrib. Mineral. Petrol.*, *58*, 63–81.

Perelló, J., A. Razique, J. Schloderer, and A. Rehman (2008), The Chagai porphyry copper belt, Baluchistan Province, Pakistan, *Econ. Geol.*, *103*, 1583–1612.

Plank, T. (2005), Constraints from thorium/lanthanum on sediment recycling at subduction zones and the evolution of the continents, *J. Petrol.*, *46*, 921–944.

Plank, T., and C. H. Langmuir (1998), The chemical composition of subducting sediment and its consequences for the crust and mantle, *Chem. Geol.*, *145*, 325–394.

Platt, J. P., J. K. Leggett, J. Young, H. Raza, and S. Alam (1985), Large-scale sediment underplating in the Makran accretionary prism, southwest Pakistan, *Geology*, *13*, 507–511.

Prelević, D., and I. Seghedi (2013), Magmatic response to the post-accretionary orogenesis within the Alpine-Himalayan belt-Preface, *Lithos*, *180–181*, 1–4.

Prelević, D., S. F. Foley, R. Romer, and S. Conticelli (2008), Mediterranean Tertiary lamproites derived from multiple source components in postcollisional geodynamics, *Geochim. Cosmochim. Acta*, *72*, 2125–2156.

Ramezani, J., and R. D. Tucker (2003), The Saghand region, central Iran: U-Pb geochronology, petrogenesis and implications for Gondwana tectonics, *Am. J. Sci.*, *303*, 622–665.

Regard, V., D. Hatzfeld, M. Molinaro, C. Aubourg, R. Bayer, O. Bellier, F. Yamini-Fard, M. Peyret, and M. Abbassi (2010), The transition between Makran subduction and the Zagros collision: Recent advances in its structure and active deformation, in *Tectonic and Stratigraphic Evolution of Zagros and Makran During the Mesozoic-Cenozoic, Geol. Soc. Spec. Publ.*, vol. 330, edited by P. Leturmy and C. Robin, pp. 43–64, Geol. Soc. Publ. House, Bath, U. K.

Richards, J. P., T. Spell, E. Rameh, A. Razique, and T. Fletcher (2012), High Sr/Y magmas reflect arc maturity, high magmatic water content, and porphyry Cu ± Mo ± Au potential: Examples from the Tethyan arcs of central and eastern Iran and western Pakistan, *Econ. Geol.*, *107*, 295–332.

Rudnick, R. L., and S. Gao (2003), Composition of the continental crust, in *The Crust, Treatise in Geochemistry*, vol. 3, edited by R. L. Rudnick, pp. 1–64, Elsevier, Oxford, U. K.
Saadat, S., and C. R. Stern (2011), Petrochemistry and genesis of olivine basalts from small monogenetic parasitic cones of Bazman strato-volcano, Makran arc, southeastern Iran, *Lithos*, *125*, 607–619.
Sadeghian, M., J. L. Bouchez, A. Nédélec, R. Siqueira, and M. V. Valizadeh (2005), The granite pluton of Zahedan (SE Iran): A petrological and magnetic fabric study of a syntectonic sill emplaced in a transtensional setting, *J. Asian Earth Sci.*, *25*, 301–327.
Schroder, J. W. (1944), Essai sur la structure de l'Iran, *Eclogae Geol. Helv.*, *37*, 37–81.
Seghedi, I., and H. Downes (2011), Geochemistry and tectonic development of Cenozoic magmatism in the Carpathian-Pannonian region, *Gondwana Res.*, *20*, 655–672.
Şengör, A. M. C., and B. A. Natal'in (1996), Paleotectonics of Asia: Fragments of a synthesis, in *The Tectonic Evolution of Asia*, edited by A. Yin and M. Harrison, pp. 486–640, Cambridge Univ. Press, Cambridge, U. K.
Şengör, A. M. C., D. Altlner, A. Cin, T. Ustaomer, and K. J. Hsu (1988), Origin and assembly of the tethyside orogenic collage at the expense of Gondwana land, in *Gondwana and Tethys, Geol. Soc. Spec. Publ.*, vol. 37, edited by M. G. Audley-Charles and A. E. Hallam, pp. 119–181, Blackwell Sci., Oxford, U. K.
Smith, G., L. McNeill, T. J. Henstock, and J. Bull (2012), The structure and fault activity of the Makran accretionary prism, *J. Geophys. Res.*, *117*, B07407, doi:10.1029/2012JB009312.
Smith, G. L., L. C. McNeill, K. Wang, J. He, and T. J. Henstock (2013), Thermal structure and megathrust seismogenic potential of the Makran subduction zone, *Geophys. Res. Lett.*, *40*, 1528–1533, doi:10.1002/grl.50374.
Spera, F. J., and W. A. Bohrson (2001), Energy-constrained open-system magmatic processes I: General model and energy-constrained assimilation and fractional crystallization (EC-AFC) formulation, *J. Petrol.*, *42*, 999–1018.
Stöcklin, J. (1968), Structural history and tectonics of Iran: A review, *Am. Assoc. Pet. Geol. Bull.*, *52*, 1229–1258.
Streckeisen, A. (1976), To each plutonic rock its proper name, *Earth Sci. Rev.*, *12*, 1–33.
Sun, S.-S., and W. F. McDonough (1989), Chemical and isotopic systematics in ocean basalt: Implication for mantle composition and processes, in *Magmatism in the Ocean Basins, Geol. Soc. Spec. Publ.*, vol. 42, edited by A. D. Saunders and M. J. Norry, pp. 313–345, Blackwell Sci., Oxford, U. K.
Tatsumi, Y. (1989), Migration of fluid phases and genesis of basalt magmas in subduction zones, *J. Geophys. Res.*, *94*, 4697–4707.
Thorpe, R. S. (1982), *Andesites: Orogenic Andesites and Related Rocks*, John Wiley, New York.
Tirrul, R., I. R. Bell, R. J. Griffis, and V. E. Camp (1983), The Sistan suture zone of eastern Iran, *Geol. Soc. Am. Bull.*, *94*, 134–150.
Verdant, Ph., et al. (2004), Present-day crustal deformation and plate kinematics in the Middle East constrained by GPS measurements in Iran and northern Oman, *Geophys. J. Int.*, *157*, 381–398.
Walker, R., P. Gans, M. B. Allen, J. Jackson, M. Khatib, N. Marsh, and M. Zarrinkoub (2009), Late Cenozoic volcanism and rates of active faulting in eastern Iran, *Geophys. J. Int.*, *177*, 783–805.
Whitmarsh, R. B. (1979), The Owen basin off the south-east margin of Arabia and the evolution of the Owen fracture zone, *R. Astron. Soc. Geophys. J.*, *58*, 441–470.
Wilson, M. (1989), *Igneous Petrogenesis*, Springer, Dordrecht, Netherlands.
Workman, R. K., and S. R. Hart (2005), Major and trace element composition of the depleted MORB mantle (DMM), *Earth Planet. Sci. Lett.*, *231*, 53–72.
Verdel, C., B. P. Wernicke, J. Hassanzadeh, and B. Guest (2011), A paleogene extensional arc flare-up in Iran, *Tectonics*, *30*, TC3008, doi: 10.1029/2010TC002809.
Zarrinkoub, M. H., K.-N. Pang, S.-L. Chung, M. M. Khatib, S. S. Mohammadi, H.-Y. Chiu, and H.-Y. Lee (2012), Zircon U-Pb age and geochemical constraints on the origin of the Birjand ophiolite, Sistan suture zone, eastern Iran, *Lithos*, *154*, 392–405.
Zhang, S.-Q., J. J. Mahoney, X.-X. Mo, A. M. Ghazi, L. Milani, A. J. Crawford, T.-Y. Guo, and Z.-D. Zhao (2005), Evidence for a widespread Tethyan upper mantle with Indian-Ocean-type isotopic characteristics, *J. Petrol.*, *46*, 829–858.